Ore Geology Reviews xxx (2014) xxx–xxx

Contents lists available at ScienceDirect

Ore Geology Reviews

journal homepage: www.elsevier.com/locate/oregeorev

Mineralogy of high-field-strength elements (Y, Nb, REE) in the world-class Vergenoeg fluorite deposit, South Africa

Torsten Graupner [a,*], Caroline Mühlbach [b], Ulrich Schwarz-Schampera [a], Friedhelm Henjes-Kunst [a], Frank Melcher [a,d], Hennie Terblanche [c]

[a] BGR Hannover, Stilleweg 2, D-30655 Hannover, Germany
[b] Sallstr. 79, D-30171 Hannover, Germany
[c] Vergenoeg Mining Company (PTY) LTD., South Africa
[d] Chair of Geology and Economic Geology, University of Leoben, Peter-Tunnerstraße 5, 8700 Leoben, Austria

ARTICLE INFO

Article history:
Received 7 June 2013
Received in revised form 10 February 2014
Accepted 21 February 2014
Available online xxxx

Keywords:
Vergenoeg fluorite deposit
HFSE mineralogy
Sm–Nd age for fluorite

ABSTRACT

The Vergenoeg fluorite deposit in the Bushveld Complex in South Africa is hosted by a volcanic pipe-like body. The distribution characteristics, composition and formation conditions of high-field-strength element (HFSE)-rich minerals in different lithological units of the deposit were investigated by optical and cathodoluminescence microscopy, scanning electron microscopy, X-ray fluorescence, inductively-coupled plasma mass-spectrometry and electron-probe microanalysis. The Vergenoeg host rocks comprise a diverse silica-undersaturated assemblage of fayalite–magnetite–fluorite with variably subordinate apatite and mineral phases enriched in rare-earth elements (REEs). The Sm–Nd isotope systematics of the fluorite from the various lithological units of the pipe support the model that the HFSE budget of the Vergenoeg pipe was likely derived from a Lebowa-type granitic magma. Isotopically, there is no evidence for other REE sources. Formation of the pipe, including development of the fluorite mineralization, occurred within the same time frame as the emplacement of other magmatic rock units of the Bushveld Complex (Sm–Nd isochron age for fluorite separates: 2040 ± 46 Ma). Hydrothermal alteration is manifested in strongly disturbed Rb–Sr isotope systematics of the Vergenoeg deposit, but did not affect its HFSE and REE budget. Whole-rock chondrite-normalized REE + Y distribution patterns of two types were observed: (i) flat patterns characteristic of magnetite–fluorite unit, gossan, metallurgical-grade fluorite ("metspar") plugs and siderite lenses, and (ii) U-shaped patterns showing enrichment towards the heaviest REE (Tm–Lu) observed in the fayalite-rich units. Common HFSE minerals are complex Nb-rich oxides (samarskite, fergusonite), REE phosphates and fluorocarbonates. Additionally, fluocerite and REE silicates, whose identification requires further work, were found. Most of the HFSE-rich minerals are spatially associated with Fe-rich phases (e.g., pyrite, magnetite, greenalite and hematite). To a smaller extent, they are found finely disseminated or healing micro-fractures in fluorite. The whole-rock REE + Y distribution patterns of the individual lithological units are mainly controlled by the distribution of Yb-rich and Y-rich xenotime in these rocks. The common occurrence of bastnäsite-(Ce) in the gossan, "metspar" plugs and especially in the rhyolitic carapace at the pipe–wall-rock contact, controls the REE + Y distribution patterns of these rocks. HFSE minerals in the Vergenoeg pipe rocks have formed in several stages. Samarskite and coarse fluorapatite belong to the primary mineral assemblage. Fergusonite and Yb-rich xenotime formed during high- to moderate-temperature hydrothermal activity. Significant remobilization of the HFSE from the early-crystallized minerals (breakdown of fluorapatite and possibly allanite with release of REE + Y) and subsequent partial redistribution of these elements into near surface rocks are inferred. The late-stage assemblages are characterized by the presence of fine-grained REE fluorocarbonates, monazite-(Ce), monazite-(La) and xenotime-(Y).

1. Introduction

The Vergenoeg deposit is one of the largest fluorite deposits in the world, accounting for 3.4% of the total world production. The Vergenoeg Igneous Complex (Vergenoeg Volcanogenic Province; Crocker, 1985) has a fluorite resource in excess of 174 million tons at 28.1% CaF_2 and a cut-off grade of 10% CaF_2 (Fourie, 2000). A variety of studies have investigated in detail the geological setting and different lithological units of the Vergenoeg fluorite deposit, the petrogenesis of fluorite in the different rock units of the deposit, and the primary and secondary Fe-bearing phases. A number of contrasting genetic models have been proposed, including the separation of an immiscible liquid from granitic

* Corresponding author. Tel.: + 49 511 643 2569.
E-mail addresses: torsten.graupner@bgr.de (T. Graupner), caroline.muecxhlbach@gmx.de (C. Mühlbach).

http://dx.doi.org/10.1016/j.oregeorev.2014.02.012
0169-1368/

magma, magmatic–hydrothermal activity, or development of a F-rich end-member of the iron oxide copper–gold (IOCG) group associated with carbonatites (Borrok et al., 1998; Crocker, 1985; Fourie, 2000; Goff et al., 2004).

The Vergenoeg pipe represents a single volcanic edifice which in an early stage produced significant volumes of ignimbrites (Fourie, 2000). Genetically, the pipe is believed to be linked to a deeper-seated granitic source, most likely related to the Lebowa Granite Suite of the Bushveld complex (Kinnaird et al., 2004). Formation of fluorite in the Vergenoeg pipe is interpreted to have occurred in at least two different stages (Kinnaird et al., 2004 and references therein). The first and economically most important generation of fluorite most likely represents a late magmatic stage (Borrok et al., 1998; Crocker et al., 2001). During magmatic activity, the magma became increasingly enriched in Fe, F and CO_2, eventually resulting in the discharge of ash, gas and fluids enriched in these components (Fourie, 2000). Borrok et al. (1998) failed to find melt inclusions in primary ore minerals (fluorite) from below the 300-m level of the Vergenoeg pipe; however, they found abundant primary high-temperature, high-salinity aqueous inclusions and also CO_2-rich inclusions in the fluorite. They interpreted these data to support formation of the fluorite from hydrothermal fluids of magmatic origin. Hydrothermal activity in a final phase of the volcanism may have induced mobilization of the fluorite, which precipitated in the hanging wall area of the pipe (Scherhag, 1990).

In contrast to the pipe structure, mineralogy of the different rock units and fluorite formation processes, the concentration, mineralogy and distribution characteristics of minor and trace elements like Y, Nb and the rare earth elements (REE) within the "layered" pipe body are largely unknown. Furthermore, the petrogenetic aspects of the distribution of these elements have not been investigated so far. Significantly, the Vergenoeg host rocks are distinctly enriched in high-field-strength elements (HFSEs). To develop a better understanding of the ore petrography, representative samples from different lithological units and depths, collected from the open pit and from drill cores, were studied using transmitted and reflected light microscopy, combined with cathodoluminescence microscopy, scanning electron microscopy (SEM) and electron-probe microanalysis (EPMA). For bulk chemical sample characterization, X-ray fluorescence (XRF) and inductively coupled plasma mass-spectrometry (ICP-MS) were applied. The Rb–Sr and Sm–Nd isotope systematics were studied using conventional thermal-ionization mass-spectrometry (TIMS). Combined data evaluation and discussion enables a better understanding of individual processes of mineral formation in the system and contributes to the discussion on the co-enrichment of F and HFSE in the intracontinental magmatic environment.

2. Geology, mineralogy and samples

The Vergenoeg mine is located in the Kaapvaal Craton in southern Africa. Its host rocks form the roof of the ca. 2.05 Ga old Bushveld Complex, which intruded an approximately 20 km thick succession of sedimentary and volcanic rocks of the Transvaal Sequence (Eriksson et al., 1995). The Vergenoeg Igneous Complex comprises pyroclastic and shallow-water sedimentary rocks. It overlies the Klipnek member of the Rooiberg rhyolite and surrounds the Vergenoeg pipe (Goff et al., 2004). The Vergenoeg pipe intruded rhyolites of the uppermost unit of the Rooiberg Group (Fig. 1) which is altered in the periphery of the pipe. The volcanic Rooiberg Group has been dated to 2061 ± 2 Ma (Walraven, 1997; Armstrong et al., unpublished, cited in Rajesh et al., 2013). Kinnaird et al. (2004) and others assumed that the rocks of the Vergenoeg volcanic pipe developed from a deeper seated granitic source likely related to the Lebowa Granite Suite, which also forms part of the Bushveld Complex. The Lebowa Suite, which intruded volcanics of the Rooiberg Group, and genetically related rhyolites were dated at 2054 ± 2 Ma (Dorland et al., 2006; Harmer and Armstrong, 2000; Scoates et al., 2012; Walraven and Hattingh, 1993). An up-to-date compilation of precise age data for the different magmatic rocks of the Bushveld Complex is given in Rajesh et al. (2013).

The Vergenoeg magnetite–fluorite–fayalite deposit is a pipe-like body (Goff et al., 2004) resembling a tapering funnel in cross section measuring 600 m (E–W) × 900 m (N–S) at the present erosion level. The body is believed to show vertical zoning with respect to lithological assemblages. Four graditional hypogene units of hematite–fluorite (gossan), magnetite–fluorite, magnetite–fayalite and fayalite (see Fig. 1) have been defined from top to bottom (Fourie, 2000). Siderite and metallurgical-grade fluorite ("metspar") lenses (plugs) occur as massive, plume-shaped bodies distributed irregularly throughout all lithological units.

According to Borrok et al. (1998), the Vergenoeg pipe is composed of (i) early-stage minerals representing the primary pipe-forming assemblage and (ii) later alteration minerals that are assigned to two secondary assemblages, and were formed by alteration and weathering of the primary assemblage. According to these authors, the lower part of the pipe contains a significant proportion of the primary assemblage, whereas its upper part is clearly dominated by the secondary assemblages. Minerals rich in HFSE (Y, Nb and REE) have formed during all stages.

Petrographic studies of Schütte (2005) and the present work suggest that the *primary mineral assemblage* mainly consists of fayalite, coarse-grained magnetite I (sometimes Ti-rich) and fluorite. Subordinate apatite and Nb–REE minerals also occur. Borrok et al. (1998) state that allanite $[(Ce,Ca,Y)_2(Al,Fe^{2+},Fe^{3+})_3(SiO_4)_3(OH)]$ is the most common REE-bearing mineral in the primary assemblage. However, we did not find allanite in our samples.

The *secondary assemblages* partly replace the primary assemblage (Borrok et al., 1998; Crocker, 1985). The earliest secondary minerals to form were amphibole (e.g., ferroactinolite/grunerite; Borrok et al., 1998), fine-grained magnetite II and minor quartz, which represent higher-temperature alteration products. Hydrothermal (~300 °C) and low-temperature weathering-related minerals include greenalite $[Fe_{2-3}(Si_2O_5)(OH)_4]$, hematite, Fe oxyhydroxides, pyrosmalite-(Fe) $[(Fe,Mn)_8((OH,Cl)_{10}/Si_6O_{15})]$, siderite, pyrite and quartz with minor fluorite, sulfides (arsenopyrite, sphalerite, various Cu sulfides), apatite and cassiterite and replace all pre-existing minerals. Furthermore, a wide variety of secondary REE minerals occur in these assemblages.

Thirty samples were collected from the Vergenoeg open pit, as well as from drill cores Kl24 (central pipe), Kl15, Kl26–28, and Kl48 (Fig. 1). Samples as large as possible were selected (up to 2500 g) due to the heterogeneous and pegmatoidal nature of the pipe rocks. Twenty-seven polished thin sections and five polished blocks were prepared for investigation by transmitted and reflected light, cathodoluminescence (CL) microscopy, SEM, EPMA and laser-ablation ICP-MS (LA–ICP-MS). Bulk-rock analyses by XRF and ICP-MS were performed on 30 samples. Additionally, hand-picked fluorite separates of selected samples were investigated for minor and trace element composition by ICP-MS and for Rb–Sr and Sm–Nd isotope compositions by TIMS. The purity of the separates is estimated to be >95% fluorite.

3. Analytical methods

Cathodoluminescence microscopy was performed using a "hot-cathode" CL microscope (Simon-Neuser HC2-LM; Neuser et al., 1995) operated at 14 kV and a current density of ~10 mA/mm^2. To prevent any build-up of electrical charge, the thin-sections were coated with carbon. Luminescence images were captured 'on-line' using a digital video camera attached to the system.

Scanning electron microscopy investigations were carried out using a Quanta 600 FEG system (FEI Company) equipped with an EDX detector (Apollo XL Silicon Drift Detector; EDAX-AMETEK) for semi-quantitative element analysis.

Electron-probe microanalysis was performed on carbon-coated sections using a Cameca SX-100 microprobe. About 250 analyses of

Please cite this article as: Graupner, T., et al., Mineralogy of high-field-strength elements (Y, Nb, REE) in the world-class Vergenoeg fluorite deposit, South Africa, Ore Geol. Rev. (2014), http://dx.doi.org/10.1016/j.oregeorev.2014.02.012

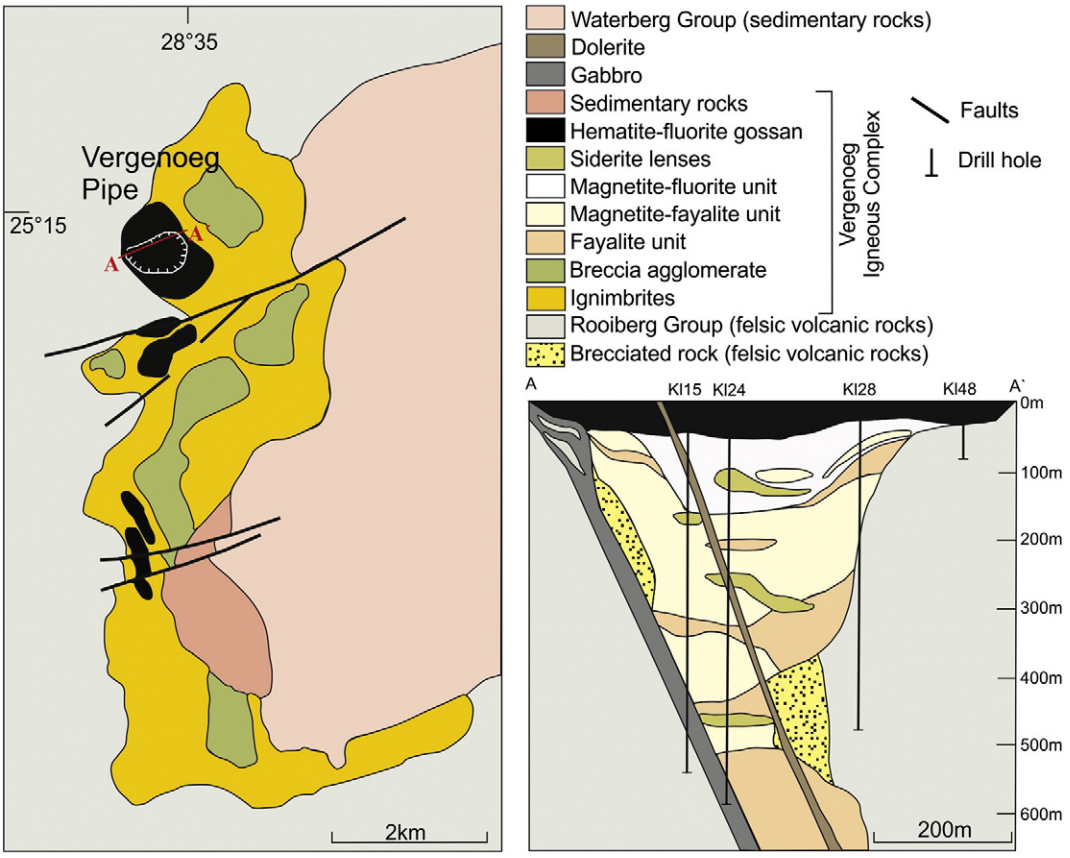

Fig. 1. Geological overview of the Vergenoeg Igneous Complex modified after Goff et al. (2004). The right sketch shows a cross-section of the Vergenoeg pipe with the distribution of the lithological units and the position of the studied drill holes.

HFSE-enriched minerals in 12 samples were obtained. The operating conditions for the measurements of the selected 42 elements were: an accelerating voltage of 15 kV and a beam current of 40 nA. Mineral and synthetic standards were used and data were obtained using a TAP crystal for Si Kα, Na Kα, Mg Kα, Al Kα, Sr Lα, and As Lα, a LLiF crystal for La Lα, Nd Lα, Sm Lβ1, Gd Lβ1, Ho Lβ1, Tm Lβ2, Lu Lα, Mn Kα, Cu Kα, Co Kα, W Lα, Ce Lα, Pr Lβ1, Eu Lβ2, Tb Lα, Dy Lβ1, Er Lα, Yb Lα, Fe Kα, Ni Kα, and Ba Lα, an LPET crystal for Ca Kα, Y Lα, P Kα, K Kα, Cl Kα, S Kα, Ti Kα, U Mα, Th Mα, Pb Mα, Nb Lα, and Zr Lα and a PC0 crystal for F Kα. The measurement times ranged between 10 and 30 s. Limits of detection (LODs) under the applied measurement conditions were: 200–400 ppm for K, Cl, Ca, S, Ti, Sr, Si, Mg, As, P, F, Al, and Na; 600–900 ppm for Pb, Nb, Mn, Fe, Y, Co, U, Th, and Ni; 900–1300 ppm for Ce, Cu, Zr, and Ba; 1600 ppm for La, and Nd; 1850–2150 ppm for Yb, Tb, Lu, Pr, Gd, and Er; 2400 ppm for Sm; 2700 ppm for Dy; 3400 ppm for Ho; 4800 ppm for Eu; 5900 ppm for W; and 6700 ppm for Tm. Relative standard deviations are 7–13% for most elements. The presence of Ta in HFSE-bearing minerals (e.g., Nb-rich complex ABO_4 minerals) was checked using several qualitative wavelength-dispersive X-ray scans; however, a Ta Lα signal was not observed in any of the cases indicating very low concentrations of this element (probably always below its LOD). In this work, La to Sm are referred to as light REE (LREE), (Eu) Gd to Ho as middle REE (MREE), and Er to Lu as heavy REE (HREE).

Laser-ablation ICP-MS analysis was carried out to determine the concentrations of REE and other trace elements in fluorite using a UP193FX New Wave research excimer laser coupled to an Agilent 7500i quadrupole ICP-MS instrument at the University of Erlangen-Nürnberg. Argon was used as a carrier gas. The spot size was 25 μm. The glass reference material NIST SRM 612 with the values of Pearce et al. (1997) was used for external calibration. Calcium was used as an internal standard (for details, see Graupner et al., 2010).

For *XRD analysis*, a PANalytical X'Pert PRO series automated powder diffractometer was employed, which uses Cu radiation (Kα line with a mean wavelength of 1.542 Å) operated at 40 kV and 30 mA, and glancing angles 2θ between 2° and 85°. For evaluation of the data the software package HighScore Plus linked with a PDF2 database was employed.

Bulk rock analysis was performed by XRF and ICP-MS techniques. *XRF analysis* was performed using two PANalytical Axios PW 2400 spectrometers. For *ICP-MS analysis*, about 100 mg of powdered sample was dissolved in screw-top Savillex™ beakers. Silicate-rich samples were dissolved with 0.5 ml HNO_3 plus 8 ml HF. After dissolution, the solutions were evaporated to dryness. Fluorite samples without significant silicate contents were dissolved with 8 ml 6.1 N HCl. The solutions were centrifuged and evaporated to dryness. Both evaporates were dissolved in HNO_3 and aliquots corresponding to about 4 mg of sample prepared for ICP-MS measurement. Element concentrations were determined using an Agilent 7500ce instrument equipped with an autosampler (for details, see Estrada et al., 2012).

For *Rb–Sr and Sm–Nd isotope analysis* by TIMS, the powdered fluorite separates were digested in splits of about 100 mg each using 0.5 ml HNO_3 plus 5 ml HF in screw-top Savillex™ beakers under clean-air conditions. Sm–Nd analysis was performed in duplicate in order to detect variations in element concentrations and isotope compositions likely related to variable amounts of REE mineral impurities. Rb–Sr and Sm–Nd isotope tracers for isotope dilution analysis were added prior to analysis. Element separation was done following conventional ion-exchange techniques (Corvino and Henjes-Kunst, 2007). Isotope composition of Sr, Sm and Nd was determined using a ThermoFinnigan TRITON TIMS instrument, whereas Rb was measured using a Finnigan MAT 261 TIMS instrument. Analytical details of the analysis are similar to those given in Estrada et al. (2012). Uncertainties are 0.0025% for $^{87}Sr/^{86}Sr$ and $^{143}Nd/^{144}Nd$ and 0.5% for $^{87}Rb/^{86}Sr$ and $^{147}Sm/^{144}Nd$,

Please cite this article as: Graupner, T., et al., Mineralogy of high-field-strength elements (Y, Nb, REE) in the world-class Vergenoeg fluorite deposit, South Africa, Ore Geol. Rev. (2014), http://dx.doi.org/10.1016/j.oregeorev.2014.02.012

respectively. Repeated measurements of the NBS SRM 987 Sr standard gave an $^{87}Sr/^{86}Sr$ ratio of 0.710196 ± 4 (n = 3). An Nd element standard (Merck™) run in the course of the sample measurements yielded $^{143}Nd/^{144}Nd = 0.512404 \pm 4$ (n = 2) which corresponds to $^{143}Nd/^{144}Nd = 0.511854$ for the LaJolla Nd standard (cross-calibrated in the BGR). The geochemical reference material AGV-2 analyzed routinely with the fluorite samples yielded $^{87}Sr/^{86}Sr = 0.703922 \pm 13$ (n = 2) and $^{143}Nd/^{144}Nd = 0.512785 \pm 6$ (n = 2). All errors are quoted at the two-sigma level unless otherwise stated. Isochron calculation and its graphical presentation were performed using Isoplot 3.6 (Ludwig, 2008).

4. Results

4.1. Bulk rock major and trace element geochemistry

Bulk rock XRF data for typical samples of each lithological unit are given in Table 1. Minor and trace elements determined by ICP-MS that are relevant to our discussion of the distribution and genesis of HFSE minerals, are also provided in Table 1. The major element geochemistry of the different lithological units (except the "metspar" plugs) is characterized by low to moderate SiO_2, very low Al_2O_3 and high to very high Fe_2O_3 and CaO (CaF_2) concentrations. The P_2O_5 values range from <0.01 to 1.31 wt.%, whereas TiO_2, Na_2O and K_2O are generally low. Silica is predominantly bound in primary fayalite, as well as secondary greenalite, pyrosmalite-(Fe) and quartz. Iron oxide is concentrated in primary fayalite and magnetite, as well as in secondary greenalite, pyrosmalite-(Fe), various Fe oxyhydroxides, Fe sulfides and Fe carbonate (siderite lenses). Calcium is mainly incorporated in fluorite and, subordinate, in apatite. Phosphate-rich minerals are represented by apatite (primary and secondary) and REE phosphates.

Uranium and Th values are generally high in the Vergenoeg pipe rocks and reach their maximum values of 384 ppm and 51.7 ppm (not included in Table 1), respectively, in the magnetite–fluorite unit. The highest U and Th values for the fayalite and magnetite–fayalite units were 16.5 ppm and 3.5 ppm, respectively.

Niobium is high in the pipe rocks, with the highest Nb contents found in samples from the hematite–fluorite gossan and magnetite–fluorite unit (54–472 ppm; mean 186 ppm (for eight samples)). Niobium contents in fayalite and magnetite–fayalite units range from 20 to 168 ppm. Tantalum is always low at Vergenoeg (0.01–2.21 ppm).

The concentrations of REE and Y are commonly high in the pipe rocks. The total REE + Y concentrations reach 1.6 wt.%, with the highest values determined in the hematite–fluorite gossan and magnetite–fluorite unit. In rhyolite from the gossan–wall-rock contact zone (marginal zone of the pipe body), extreme total REE + Y values of up to 30 wt.% were found locally. Rocks from all units of the pipe show

Table 1
Bulk rock geochemical analyses of the Vergenoeg rocks.

Sample	Magnetite–fayalite unit		Fayalite unit		Siderite lenses		Magnetite–fluorite unit	Hematite–fluorite gossan	"Metspar" plugs	
	SA09-113	SA09-114	SA09-123	SA09-125	SA09-111	SA09-118	Ver12-3b	SA09-106	SA09-120	SA09-121
wt.%										
SiO_2	23.56	23.25	12.34	21.32	1.66	0.55	1.77	29.41	0.32	0.11
TiO_2	0.09	0.01	0.19	0.13	0.01	0.003	0.08	0.16	<0.001	<0.001
Fe_2O_3	65.89	60.56	39.58	69.82	45.56	65.59	50.29	14.99	0.28	1.99
Al_2O_3	0.08	0.07	0.09	0.10	0.19	<0.05	0.37	0.56	<0.05	<0.05
MnO	1.41	1.10	0.74	0.72	1.78	2.73	0.08	0.01	<0.001	0.04
MgO	0.51	0.42	0.22	0.40	0.24	0.27	0.03	0.03	0.03	0.05
(CaO)	0.71	9.98	29.35	4.90	23.23	0.69	33.60	39.91	72.24	70.83
CaF_2	0.99	13.90	40.86	6.82	32.34	0.96	46.78	55.57	100.58	98.62
Na_2O	<0.01	<0.01	<0.01	<0.01	<0.01	<0.01	<0.01	<0.01	0.03	0.02
K_2O	0.01	0.01	0.03	0.01	0.03	0.01	<0.005	0.11	<0.005	<0.005
P_2O_5	0.02	0.01	0.04	0.09	0.02	0.02	0.46	0.12	0.01	0.01
Total[a]	100.08	102.00	103.00	101.35	103.31	100.00	102.68	103.02	101.65	102.08
ppm										
Rb	3.36	1.48	1.52	0.58	2.20	0.66	10[b]	11.00	0.79	0.21
Sr	11.00	5.76	17.80	4.45	10.20	3.19	42[b]	21.60	20.30	26.70
Ba	7.71	6.05	12.10	3.47	13.60	9.25	<47[b]	61.10	6.81	2.19
V	2.35	0.25	2.63	4.55	0.57	0.51	<7[b]	26.90	0.13	0.23
Cr	0.71	0.41	1.59	0.78	0.24	0.15	<5[b]	12.20	0.21	0.36
Co	21.80	14.10	6.93	13.90	24.30	12.40	9[b]	12.00	0.17	2.20
Th	0.21	0.05	3.49	1.35	0.27	0.05	33.60	8.37	0.02	0.01
U	1.35	0.93	4.31	16.50	1.44	0.24	145.00	7.80	0.79	0.61
Zr	14.10	6.29	11.80	9.20	0.80	0.16	18[b]	20.40	0.26	0.10
Hf	0.65	0.19	0.38	0.37	0.04	0.01	<11[b]	0.62	0.03	0.02
Nb	59.30	59.60	63.80	86.00	6.10	1.01	283[b]	119.00	1.34	0.77
Ta	1.10	0.65	1.35	1.19	0.08	0.01	<9[b]	0.84	0.04	0.01
Y	124.00	286.00	1070.00	376.00	549.00	40.70	1490[b]	1200.00	2320.00	1780.00
La	23.50	4.91	123.00	87.80	58.60	3.81	390.00	226.00	66.50	32.10
Ce	46.60	14.70	229.00	266.00	113.00	9.86	1150.00	466.00	135.00	81.00
Pr	4.53	2.35	25.20	38.60	13.50	1.34	153.00	56.00	18.50	12.30
Nd	14.10	11.00	85.30	143.00	53.40	5.28	590.00	198.00	87.60	63.40
Sm	2.89	3.34	21.90	34.10	13.60	1.90	136.00	37.60	28.80	22.50
Eu	0.22	0.13	1.03	0.79	0.57	0.12	4.54	2.95	0.90	0.69
Gd	0.88	4.38	28.70	21.60	16.50	2.80	80.10	16.80	47.10	36.80
Tb	0.72	1.05	5.71	5.95	3.29	0.64	10.10	8.96	9.63	7.59
Dy	8.01	10.30	47.60	42.80	26.40	4.72	59.30	76.10	78.30	61.30
Ho	3.39	3.58	14.00	10.40	6.84	1.11	12.80	19.00	21.30	16.70
Er	23.30	19.90	60.70	41.00	25.10	3.95	41.50	66.20	75.80	56.90
Tm	8.31	6.23	14.40	9.44	4.58	0.85	6.36	11.60	10.30	8.42
Yb	107.00	74.30	153.00	93.10	35.30	7.95	41.80	79.90	59.40	50.70
Lu	25.00	15.10	31.10	18.40	5.10	1.42	5.26	9.88	7.08	6.23

Major elements determined by XRF, minor and trace elements (Rb to Lu) determined by ICP-MS.
[a] Total of major element oxides determined by XRF (LOI data not shown); includes Ca as CaF_2.
[b] Trace element data determined by XRF.

Please cite this article as: Graupner, T., et al., Mineralogy of high-field-strength elements (Y, Nb, REE) in the world-class Vergenoeg fluorite deposit, South Africa, Ore Geol. Rev. (2014), http://dx.doi.org/10.1016/j.oregeorev.2014.02.012

a more or less pronounced negative Eu anomaly and a weak to moderate positive Y anomaly; no Ce anomaly was observed in any of the data sets.

4.2. Ore mineralogy and geochemistry

4.2.1. Fluorite

Fluorite is present in variable quantities throughout the Vergenoeg pipe. With increasing depth, its abundance decreases. In contrast, an increase in the content of iron-bearing minerals (mainly magnetite and fayalite) was observed with increasing depth. Fluorite occurs in both massive and disseminated forms, as well as in late veinlets and open-space fillings. The mineral is commonly colorless to pale greenish in hand specimen; however, fluorite with purple color occurs locally. Randomly distributed, mostly euhedral fluorite grains and grain aggregates (sometimes >50 mm in size) are common in the hematite–fluorite gossan and magnetite–fluorite unit. Interstitial fluorite occurs mainly in the fayalite-bearing units of the pipe. Fluorite overgrowing late-stage REE minerals in cavities (or pseudomorphs) occurs in minor quantities in the pipe rocks. Inclusions of small REE minerals are present in minor amounts in fluorite grains and aggregates in all rock types.

Different fluorite generations are distinguished by transmitted light and CL microscopy (Fig. 2a–c). All fluorite types investigated show bright to dark bluish CL colors. Frequently, fluorite grains are dominated by homogeneous bright bluish CL colors, but also show fracture-related multiple bands or spot-like areas (both having dark bluish CL; Fig. 2a), as well as anastomosing textures with different shades of bluish CL color or zoning in euhedral to subhedral grains (Fig. 2b). Fluorite with dark bluish CL and possible growth zoning (Fig. 2c) is rare in the studied samples. In the siderite lenses, at least two generations of fluorite are distinguished using CL microscopy: (i) subhedral to euhedral coarse grains and (ii) commonly finer-grained fluorite, arranged interstitially with respect to carbonate, or forming large aggregates. The fine grain size of fluorite in these aggregates is visible in CL images only. The latter fluorite aggregates also contain corroded elongated fragments of zoned, originally coarse fluorite. The fragments display bright bluish CL colors, whereas the patchy appearing, fine-grained fluorite predominantly has dark bluish CL.

The trace element composition of fluorite was determined using ICP-MS analysis of hand-picked fluorite separates (three sub-samples per rock sample) and by LA–ICP-MS of fluorite grains in polished sections. The ICP-MS data for each set of three sub-samples indicate rather uniform distributions of HFSE (Nb, Ta, REE and Y) and of impurities (especially Fe-bearing phases; results not shown) in the separates. The samples from the different lithological units show similar chondrite-normalized REE patterns and mostly differ by slight shifts of the patterns along the abscissa (Fig. 3). However, it should be noted that the three sub-samples deriving from one of the two fayalite unit samples are slightly enriched in the heaviest REE (Tm–Lu, black lines in Fig. 3) and show lower Er/Yb ratios compared to all other fluorite samples.

Laser-ablation ICP-MS was applied to resolve compositional variations in closely intergrown types of fluorite. Representative trace element compositions of the three fluorite types distinguishable in the Vergenoeg samples (types Ia, Ib and II) are listed in Table 2. Fluorite of type Ia is most widely distributed in the magnetite–fayalite unit, fayalite unit, hematite–fluorite gossan, and "metspar" plugs. Types Ib (coarse-grained fluorite) and II (predominantly finer-grained fluorite in CL imaging) occur restricted to the siderite lenses.

Fluorite of type Ia contains the highest REE + Y concentrations among the studied samples (REE + Y = 1250–5290 ppm with a mean of 2554 ppm; Y = 950–4390 ppm with a mean of 2018 ppm; n = 36) of all types. Furthermore, it shows elevated Sr values (24.6–58.8 ppm; mean 34.1 ppm). The Y anomalies quantified as the Y/Y* ratio = $[Y_N / (0.5 * (Dy_N + Ho_N))]$, Y/Ho ratios, Tb/La atomic ratios and Tb/Ca atomic ratios are in the ranges 2.38–5.18, 60–137, 0.03–0.45 and 1.29×10^{-6}–7.81×10^{-6}, respectively.

Compared to type Ia, fluorite Ib contains lower REE concentrations (REE + Y = 130–1720 ppm; Y = 66–1290 ppm; n = 6) and also somewhat lower Sr concentrations (21.8–29.1 ppm; mean 25.4 ppm); however, its Y/Y*, Y/Ho, Tb/La and Tb/Ca values (1.85–3.60, 57–93, 0.04–0.25, 2.58×10^{-7}–3.12×10^{-6}, respectively) are rather similar to type Ia.

Fluorite II strongly differs from type Ia and Ib fluorites in trace element composition. Fluorite II has relatively low Sr concentrations (11.8–27.5 ppm; mean 18.6 ppm) and shows an extremely strong

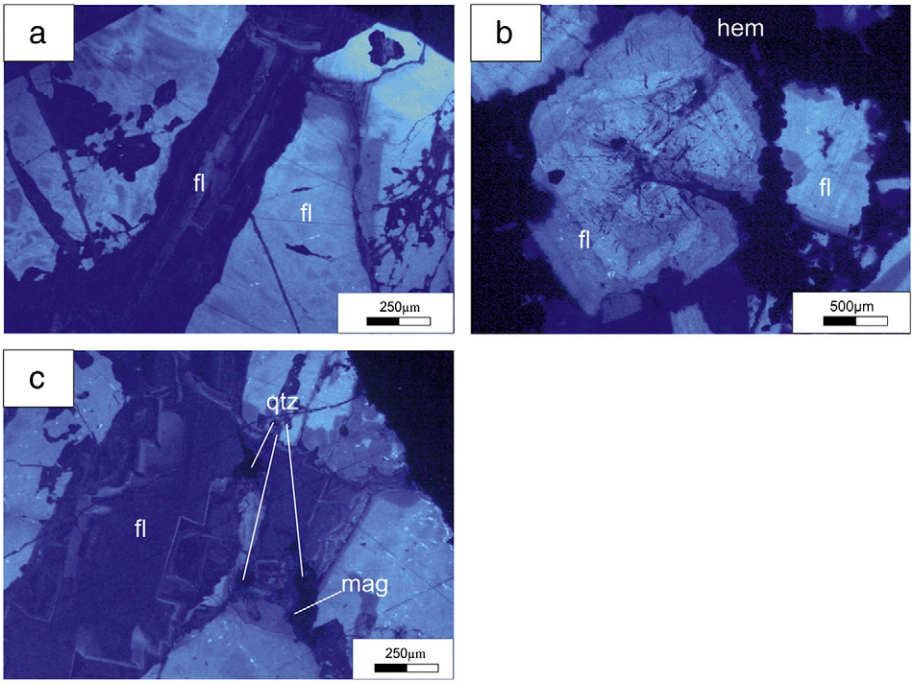

Fig. 2. Cathodoluminescence (CL) photomicrographs of fluorite from different lithological units in the Vergenoeg pipe. (a) Sample from a "metspar" plug showing replacement or overprinting of early fluorite starting from a micro-fracture. (b) Sample from the hematite–fluorite gossan with zoned fluorite grains enclosed by late hematite. (c) Sample from a "metspar" plug showing two varieties of fluorite separated by quartz and magnetite. Abbr.: fl: fluorite; hem: hematite; mag: magnetite; qtz: quartz.

Please cite this article as: Graupner, T., et al., Mineralogy of high-field-strength elements (Y, Nb, REE) in the world-class Vergenoeg fluorite deposit, South Africa, Ore Geol. Rev. (2014), http://dx.doi.org/10.1016/j.oregeorev.2014.02.012

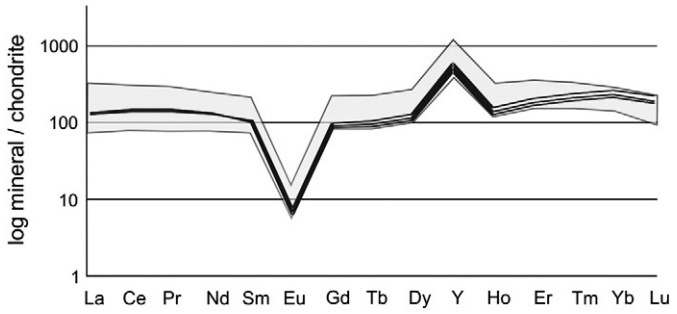

Fig. 3. Chondrite-normalized REE patterns of fluorite separates from Vergenoeg. The shaded field shows the overall variability of all fluorite separate samples from all studied lithological units. For details on the individually shown three subsamples of one sample (black lines) see text.

positive Y anomaly ($Y/Y^* = 7.19–14.5$). The Y/Ho ratio is very high with values ranging from 194 to 406. Furthermore, fluorite II contains low REE concentrations (REE + Y = 129–1370 ppm; n = 9). The Tb/La atomic ratios range from 0.09 to 0.54, whereas Tb/Ca atomic ratios range from 9.04×10^{-8} to 1.50×10^{-6}.

4.2.2. Apatite

Coarse-grained primary euhedral apatite occurs intergrown with coarse-grained magnetite I and fayalite, which is more or less completely replaced by serpentine, pyrosmalite-(Fe) and Fe oxyhydroxides, in samples from the magnetite–fayalite unit (Fig. 4). The apatite aggregates are often cross-cut by veinlets of secondary pyrosmalite-(Fe) and/or contain numerous elongated inclusions of secondary Fe minerals. Secondary apatite grains are commonly small and occur in clusters.

Backscattered electron (BSE) images of primary apatite grains show an intensely developed patchy or band-like internal texture with dark and bright domains resulting from chemical overprinting of the mineral. The internal domains of individual grains that appear brighter in BSE images give a higher Ce signal in energy-dispersive X-ray spectra compared to the darker marginal domains (Fig. 4). Within the secondary Fe minerals surrounding the apatite grains, as well as in adjacent

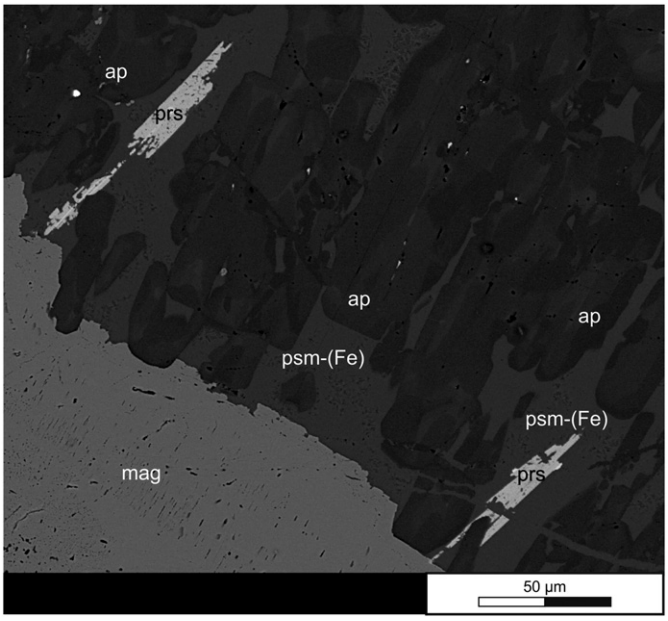

Fig. 4. Back-scattered electron (BSE) image of apatite from the magnetite–fayalite unit. The image illustrates a patchy or band-like internal texture resulting from hydrothermal overprinting. The brighter internal domains of the apatite grains have higher REE (Ce) contents compared to the darker marginal domains. Abbr.: ap: apatite; mag: magnetite; psm-(Fe): pyrosmalite-(Fe); prs: parisite.

pseudomorphs after fayalite, numerous aggregates of needle-like REE fluorocarbonate grains [bastnäsite-(Ce) $Ce(CO_3)F$, parisite-(Ce) $Ca(Ce,La)_2(CO_3)_3F_2$] occur. The parisite shown in the lower right area of Fig. 4 is cut by a pyrosmalite-(Fe) veinlet and its fragments are displaced.

The primary apatite has F and Cl contents of 3.7–3.9 wt.% and <0.1 wt.%, respectively; the SrO and MgO contents are always below their LOD. Consequently, the composition of the primary apatite is close to the fluorapatite end-member. Concentration of total rare earth oxides (TREOs) + Y_2O_3 in some primary apatite grains from the

Table 2
Laser-ablation ICP-MS data of fluorite.

Fluorite type	Ia		Ib		II	
Sample	Fayalite unit	Hematite–fluorite gossan	Siderite lenses			
ppm	SA09-123	SA09-104	SA09-111/8	SA09-111/11	SA09-111/1	SA09-111/50
Rb	0.48	0.15	0.69	0.26	0.81	0.84
Sr	34.90	36.70	21.80	27.90	14.00	14.90
Th	0.04	0.02	<0.004	<0.004	0.02	0.07
U	0.18	0.23	0.03	0.03	<0.004	<0.004
Zr	<0.007	<0.012	0.03	<0.007	<0.004	<0.010
Hf	<0.005	<0.010	<0.010	<0.009	<0.005	0.02
Y	2320.00	2850.00	695.00	817.00	830.00	511.00
La	30.30	49.40	11.50	12.40	5.29	5.06
Ce	85.30	131.00	32.10	33.90	12.20	10.50
Pr	12.80	19.80	5.35	6.48	2.08	1.98
Nd	71.70	101.00	29.90	33.30	9.62	11.10
Sm	24.40	36.60	9.91	11.60	3.64	3.78
Eu	0.80	0.81	0.41	0.47	0.23	0.24
Gd	44.80	63.50	15.70	18.40	8.79	7.29
Tb	8.36	11.00	3.19	3.60	1.96	0.97
Dy	70.70	102.00	28.50	32.30	12.60	7.44
Ho	19.90	26.20	7.71	8.76	3.10	1.90
Er	64.70	86.60	28.80	33.70	11.30	5.72
Tm	9.96	13.00	4.80	5.80	1.82	0.79
Yb	59.50	78.40	35.80	41.70	13.10	7.87
Lu	7.06	8.22	3.93	4.49	1.58	0.97
REE + Y total	2832	3583	913	1064	917	577
Y/Ho	116.7	109.0	90.1	93.3	267.7	268.9
Y/Y*	4.59	4.11	3.48	3.60	9.88	10.11

$Y/Y^* = [Y_N / (0.5 * (Dy_N + Ho_N))]$.

Please cite this article as: Graupner, T., et al., Mineralogy of high-field-strength elements (Y, Nb, REE) in the world-class Vergenoeg fluorite deposit, South Africa, Ore Geol. Rev. (2014), http://dx.doi.org/10.1016/j.oregeorev.2014.02.012

magnetite–fayalite unit are in the range from 2.64 to 2.90 wt.%. However, only La_2O_3–Nd_2O_3 (1.80–2.32 wt.%) and Y_2O_3 (0.58–0.84 wt.%) contents were detectable with EPMA; all other REE were below their LOD.

4.2.3. Mineralogy of high-field-strength elements (Y, Nb, REE)

The HFSE-rich mineral phases within the Vergenoeg pipe generally are characterized by small grain sizes (~10 μm) and are commonly intimately intergrown with one another or with other fine-grained minerals. Thus, their precise identification by optical microscopic methods is difficult and often impossible. Fourteen polished thin sections from all major lithological units of the deposit were selected to characterize their HFSE (Y, Nb, REE) mineralization using SEM and EPMA combined with powder X-ray diffraction.

Rare-earth phosphates [xenotime-(Y) YPO_4 and monazite-(Ce) and -(La) (Ce,La)PO_4], REE fluorocarbonates [bastnäsite-(Ce), parisite-(Ce), synchysite-(Ce) and -(Y) $CaREE(CO_3)_2F$], and complex Y–REE–Nb–Ti oxides [samarskite-(Y) $(Y,Ce,U,Fe^{3+})_3(Nb,Ta,Ti)_5O_{16}$, fergusonite-(Y) $YNbO_4$] are common minerals. Additionally, fluocerite-(Ce) [$(Ce,La)F_3$], poorly characterized REE silicates and a non-stoichiometric Y-rich, Ca-bearing mineral are present. The Levinson modifiers are dropped in the subsequent text, unless the dominant REE species needs to be specified.

The Y–Nb–REE minerals are rather common in all lithological units, except for the magnetite–fayalite unit and the siderite lenses; the latter have distinctly lower concentrations of these minerals. In general, Y–Nb–REE-rich minerals are spatially associated with Fe-rich phases (e.g., pyrite, magnetite, greenalite and hematite) and, to a smaller extent, finely disseminated or healing micro-cracks in fluorite.

4.2.3.1. Rare-earth phosphates

4.2.3.1.1. Xenotime.

Xenotime is present in all investigated lithological units of the Vergenoeg pipe. Two types of xenotime grains, showing chemical and morphological differences, occur in the deposit. The first type is Yb-enriched (e.g., in the magnetite–fayalite unit with Y_2O_3 23.5–33.1 wt.% and Yb_2O_3 15.5–29.3 wt.%), and the second one is clearly Y-dominated (e.g., in the hematite–fluorite gossan with Y_2O_3 38.0–52.3 wt.% and Yb_2O_3 2.0–4.4 wt.%). Typical examples of both xenotime types are shown in Fig. 5 and their compositions are given in Table 3.

The Yb-rich xenotime was found restricted to the magnetite–fayalite and fayalite lithological units. It generally forms coarse grains dispersed in greenalite or its decay products (Fig. 5a,b), sometimes exhibiting euhedral crystal forms and occasionally with internal zoning (Fig. 5a). Aggregates composed of several coarse grains of Yb-rich xenotime are scarce. Its morphological features indicate its early crystallization. Grains composed of an Yb-rich core and Y-rich secondary rim were observed in pyrosmalite-(Fe) (Fig. 5c).

Late stage (secondary) Y-rich fine-grained xenotime occurs in all parts of the deposit including the siderite lenses and "metspar" plugs. Commonly, secondary xenotime can be found intergrown with sulfides. The Y-rich xenotime occurs in association with fluocerite. Commonly, it shows a patchy texture (Fig. 5f). In gossan samples, this variety is common in pseudomorphs, probably after fayalite. Yttrium-rich xenotime is often intergrown with fine-grained monazite (Fig. 5d). In the "metspar" plugs, Y-rich xenotime is intergrown with sulfides (e.g., pyrite, chalcopyrite and chalcocite) in healed micro-cracks cutting the fluorite (Fig. 5e). The siderite lenses exhibit a slightly greater variability with respect to the Y/Yb ratios of Y-rich xenotime, compared to the other units.

To separate the early and secondary xenotime based on the EPMA data, Er and Yb concentrations were plotted using the approach of Förster (1998) in Fig. 6. The concentrations of Er and Yb in xenotime from Vergenoeg range from 0.02 to 0.06 apfu and 0.02 to 0.34 apfu, respectively.

The field contoured with the red dashed line in Fig. 6 contains early xenotime from the fayalite and magnetite–fayalite units, which obviously share high Er and moderate to very high Yb contents. By contrast, low to moderate Er contents and low Yb contents are typical of all secondary Y-rich xenotime grains and xenotime rims around the early Yb-rich xenotime in the fayalite unit (Fig. 6, orange-contoured field). Samples from the hematite–fluorite gossan, magnetite–fluorite unit, siderite lenses and "metspar" plugs plot entirely in the field of the Y-rich secondary xenotime.

4.2.3.1.2. Monazite.

Monazite was found in most of the investigated units of the Vergenoeg pipe, with the exception of the magnetite–fayalite unit. Commonly, monazite-(Ce) is anhedral, very fine-grained and closely intergrown with secondary Y-rich xenotime (Fig. 5d). In the gossan, small grains of monazite-(Ce) are intergrown with bastnäsite-(Ce) in pseudomorphs after fayalite (e.g., Fig. 7a). Monazite-(La) occurs locally in hematite aggregates intergrown with fine-grained fluorite.

Less commonly, fine-grained monazite-(Ce) cements void spaces close to coarse Yb-rich xenotime in the fayalite unit. Fig. 7b shows small monazite-(Ce) aggregates in an early euhedral magnetite I grain outlining finger-like areas of replacement; magnetite I is replaced by various Fe oxyhydroxides (magnetite–fluorite unit). The occurrence of all monazite in areas strongly affected by late fluid activity (in pseudomorphs, replacement areas, as trails outlining healed fractures) supports the formation of this mineral at a late (secondary) mineralization stage (Fig. 7b).

The Nd_2O_3 vs. La_2O_3 plot (Fig. 8) indicates that the highest Nd concentrations in monazite-(Ce) from Vergenoeg occur in the magnetite–fluorite unit (up to ~17 wt.% Nd_2O_3). Monazite-(Ce) from the fayalite unit has a wide range of Nd/La ratios (0.5–2.1). Finally, two groups of monazite occur in the hematite–fluorite gossan: an apparently more common type 1 [monazite-(Ce) and monazite-(La) with Nd/La = 0.1–0.2] and monazite-(Ce) of type 2 with higher Nd/La ratios (1.6–1.7).

4.2.3.2. Rare-earth fluorocarbonates.

In one sample from the magnetite–fayalite zone, possibly early-stage coarse synchysite-(Ce) is overgrown by a thin rim (up to 10 μm wide) of bastnäsite-(Ce). REE fluorocarbonates formed predominantly during late stages of the formation of the Vergenoeg deposit, as indicated by their modes of occurrence (see below). They are widespread in samples from the gossan, "metspar" plugs and rhyolite [bastnäsite-(Ce); according to XRD data] from the pipe–wall-rock contact zone. Samples from the siderite lenses are devoid of REE fluorocarbonates; in the magnetite–fluorite unit, bastnäsite is present locally. Rare-earth fluorocarbonates are often intergrown with monazite and Y-rich xenotime. Most fluorocarbonates contain Ce as the predominant REE cation; yttrium-dominated fluorocarbonates are scarce (Table 3). Bastnäsite-(Ce) is the most common mineral of this group; parisite-(Ce), synchysite-(Ce) and synchysite-(Y) occur subordinately.

Late stage REE fluorocarbonates are common in pseudomorphs from the surficial parts of the deposit and generally form irregular, fine-grained aggregates (Fig. 7a). Euhedral bastnäsite also forms overgrowths on anhedral quartz, with bastnäsite crystals projecting into a cavity that was subsequently filled by late hydrothermal fluorite (inset in Fig. 7a). The secondary anhedral quartz in such pseudomorphs commonly hosts anhedral Y-rich xenotime and monazite aggregates.

Representative EPMA data for the REE fluorocarbonates are given in Table 3. In Fig. 9, the compositional variation of the REE fluorocarbonates within the Vergenoeg deposit is illustrated. In the Ce versus Ca and Y versus Ca plots (Fig. 9a–b), the predominance of Ce in the REE fluorocarbonates from Vergenoeg is evident. Only fluorocarbonates from the large "metspar" plugs contain significant amounts of Y (Fig. 9b). Fig. 9c–d indicates that the hematite–fluorite gossan hosts two chemically different types of bastnäsite-(Ce). One type shows Nd > La and occurs intergrown with Y-rich xenotime, whereas the other type has La > Nd, and is commonly intergrown with hematite and fluorite only.

Please cite this article as: Graupner, T., et al., Mineralogy of high-field-strength elements (Y, Nb, REE) in the world-class Vergenoeg fluorite deposit, South Africa, Ore Geol. Rev. (2014), http://dx.doi.org/10.1016/j.oregeorev.2014.02.012

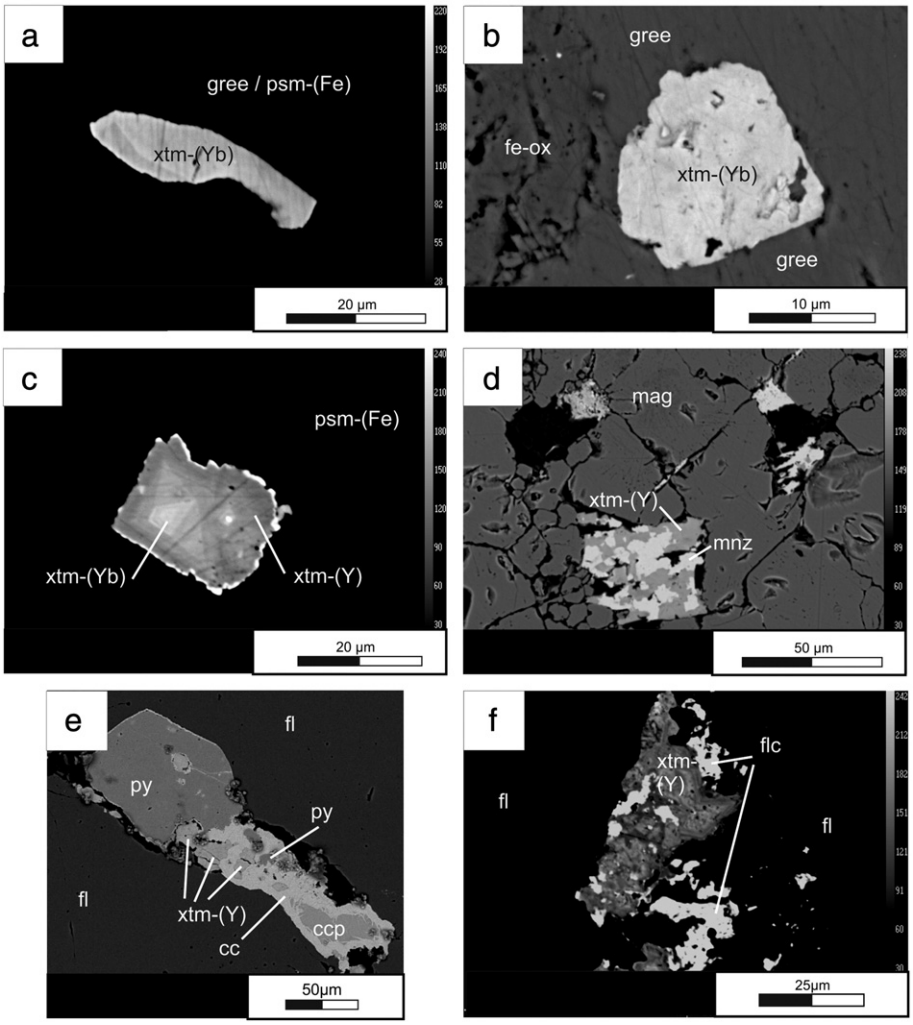

Fig. 5. BSE images of (a–c) primary Yb-rich xenotime and (d–f) secondary Y-rich xenotime from Vergenoeg. (a) Magnetite–fayalite unit: zoned subhedral Yb-rich xenotime grain in greenalite–pyrosmalite-(Fe). (b) Fayalite unit: euhedral grain of Yb-rich xenotime in greenalite. (c) Fayalite unit: zoned xenotime grain composed of an Yb-rich core and a Y-enriched secondary rim. (d) Fayalite unit: secondary Y-rich xenotime intergrown with fine-grained monazite (pseudomorph?). (e) "Metspar" plug: late Y-rich xenotime intergrown with chalcopyrite, chalcocite and pyrite in a veinlet cross-cutting fluorite. (f) "Metspar" plug: late Y-rich xenotime with patchy internal texture intergrown with fluocerite filling veinlet cross-cutting fluorite. Abbr.: cc: chalcocite; ccp: chalcopyrite; fe-ox: iron-oxyhydroxide; fl: fluorite; flc: fluocerite; gree: greenalite; mag: magnetite; mnz: monazite; psm-(Fe): pyrosmalite-(Fe); py: pyrite; xtm-(Y)/-(Yb): xenotime enriched in Y and Yb, respectively.

4.2.3.3. Rare-earth silicates.

In this study, we detected various REE-bearing silicates in the hematite–fluorite gossan, magnetite–fayalite and fayalite units and "metspar" plugs. All of them are rare and represented by small grains (<20 µm). They either occur inside of large fluorite aggregates, or are clearly confined to late, healed fractures, together with secondary Fe minerals such as pyrite, pyrosmalite-(Fe) and Y-rich xenotime. Consequently, their formation in the Vergenoeg pipe occurred probably during all mineralization stages, except the primary magmatic one. The REE silicates occur as anhedral aggregates or euhedral grains, which are internally homogeneous or partly zoned, as illustrated in Fig. 10a–b.

All REE silicates have moderate concentrations of CaO (2.2 to 9.4 wt.%); FeO reaches values up to 10.5 wt.%, but is sometimes <LOD. The REE silicates contain either high Y_2O_3 (12–31 wt.%) or high La_2O_3 and Ce_2O_3 contents (22–25 and 30–32 wt.%, respectively). Based on the EPMA data, the grains are tentatively identified as follows:

(i) Few grains of a La–Ce-rich silicate in the hematite–fluorite gossan probably represent stillwellite-(Ce) [(Ce,REE)$BSiO_5$] (Fig. 10a).

(ii) In samples from the magnetite–fayalite unit, fayalite unit and "metspar" plugs, several anhedral and euhedral grains of hingganite-(Y) [$(Y,REE)_2(Fe^{2+})Be_2(SiO_4)_2(OH)_2$] were identified. This mineral represents the most common REE silicate at Vergenoeg. It occurs in cavities in fluorite and in intersecting veinlets (Fig. 10b).

(iii) Okanoganite-(Y) [$(Na,Ca)_3(Y,REE)_{12}Si_6B_2O_{27}F_{14}$] was found in the "metspar" plugs, as grains enclosed in Fe sulfide.

4.2.3.4. Complex ABO_4 minerals. At Vergenoeg, Nb-rich Y–REE oxide minerals (Fig. 10c–f) are restricted to two of the lithological units. The empirical approach of Ercit (2005) was used to tentatively assign these minerals to the samarskite and fergusonite groups. Fig. 11 presents the analytical data.

4.2.3.4.1. Samarskite-(Y). Samarskite-(Y) is present in two samples from the magnetite–fayalite unit. Primary samarskite grains show distinct crystal faces and evidence of strong corrosion (Fig. 10c–d). Individual grains are up to 120 µm in size (much larger than REE-phosphate and REE-fluorocarbonate grains). Samarskite occurs either intergrown with apatite and coarse-grained magnetite I or is associated with secondary Fe oxides and sulfides (Fig. 10c–d).

The samarskite grains show highly irregular zoning; the zones are "patchy", but more or less continuously developed (Fig. 10c–d). The dark zones in BSE images have high FeO (up to 25 wt.%) and highly variable Nb_2O_5 (30–66 wt.%), whereas the brighter zones have rather

Please cite this article as: Graupner, T., et al., Mineralogy of high-field-strength elements (Y, Nb, REE) in the world-class Vergenoeg fluorite deposit, South Africa, Ore Geol. Rev. (2014), http://dx.doi.org/10.1016/j.oregeorev.2014.02.012

Table 3
Typical compositions of major HFSE-bearing minerals from the Vergenoeg fluorite deposit (Electron-probe microanalysis; all data in wt.%).

Mineral	Yb-rich xenotime	Yb-rich xenotime	Y-rich xenotime	Y-rich xenotime	Monazite-(Ce)	Monazite-(La)	Bastnäsite-(Ce)	Parisite-(Ce)	Synchysite-(Ce)	Synchysite-(Y)	Samarskite-(Y) (REE-rich, bright in BSE)	Samarskite-(Y) (REE-poor, dark in BSE)	Fergusonite-(Y) (Yb-rich, bright in BSE)	Fergusonite-(Y) (dark in BSE)
Sample	Fayalite unit	Magnetite–fayalite unit	Magnetite–fluorite unit	Hematite–fluorite gossan	Hematite–fluorite gossan	Hematite–fluorite gossan	Hematite–fluorite gossan	Magnetite–fayalite unit	Magnetite–fayalite unit	"Metspar" plug	Magnetite–fayalite unit	Magnetite–fayalite unit	Magnetite–fayalite unit	Magnetite–fayalite unit
	SA09-123/7	SA09-114/13	Ver12-3b/11	SA09-108/35	SA09-103/16	SA09-108/2	SA09-108/9	SA4075/2	SA4075/16	SA09-120/18	SA4075/11	SA4075/10	SA09-114/2	SA09-114/1
F	0.39	0.96	0.12	0.28	0.18		8.74	4.49	4.51	5.56				
CO_2(calc)							20.52	26.65	29.70	29.72				
P_2O_5	28.77	25.78	33.91	34.71	27.82	30.08	0.15				0.16	0.12		
As_2O_3			0.26	0.13	0.08					0.06				
Nb_2O_5											47.10	65.61	48.23	46.96
SiO_2	1.26	3.37	0.10	0.69		0.09	0.07	0.06			1.33	0.62		
FeO	2.77[a]	5.07[a]	0.19	1.43[a]	0.35	0.83	0.17	0.81			5.67	11.29	1.19	2.85
MnO		0.11[a]									1.63	6.11	0.10	0.20
CaO	0.05	0.20	0.17	0.27	0.51	0.08	1.20	11.39	19.67	18.95	1.26	0.35	1.24	1.00
TiO_2											0.36	1.31	0.10	
ZrO_2	0.35			0.31								0.13	2.39	0.54
PbO_2	0.35	0.18	0.42	0.49							0.39	0.42	0.48	0.57
ThO_2	0.13				0.24		0.44				0.63	0.37		
UO_2	0.21		0.36	0.11							5.01	1.59		1.03
Y_2O_3	32.01	28.16	43.73	50.20	0.28	0.16	0.89	0.58	2.18	14.93	15.42	5.45	19.94	21.68
La_2O_3					9.80	31.89	25.17	17.77	14.71	7.40			1.17	0.38
Ce_2O_3			0.12		34.57	30.73	35.84	34.08	27.57	16.41	0.85	0.29	1.46	3.19
Pr_2O_3					4.26	1.63	2.59	2.98	2.25	1.58	0.29			0.80
Nd_2O_3			0.27		15.59	3.38	6.04	8.17	5.55	5.39	1.52	0.51		4.40
Sm_2O_3			0.67		2.35					1.11	1.04	0.36		1.47
Gd_2O_3	0.52		2.57	1.08	1.07		0.45	0.28		1.33	1.41	0.43	0.64	1.72
Tb_2O_3			0.61								0.29	0.22		
Dy_2O_3	1.93		4.96	2.78						0.77	3.08	0.95	0.65	2.11
Ho_2O_3	1.22	0.75	1.16	0.66							0.80			
Er_2O_3	4.41	4.57	3.82	2.19							2.89	1.04	3.29	2.56
Tm_2O_3	2.03	2.39									1.35		1.47	
Yb_2O_3	17.33	23.47	4.22	2.17							4.76	1.70	15.55	5.58
Lu_2O_3	2.56	3.53	0.54	0.38							0.25	0.27	1.99	0.76
Total	96.36[b]	98.56[b]	98.23[b]	98.42[b]	97.41[b]	98.91	98.77[b]	105.38[b]	104.24[b]	101.06[b]	98.68	99.88	100.40	99.54

Empty fields: below detection limit; Eu was sought, but not detected.
[a] Contamination from host mineral (Fe oxide).
[b] Total O = F.

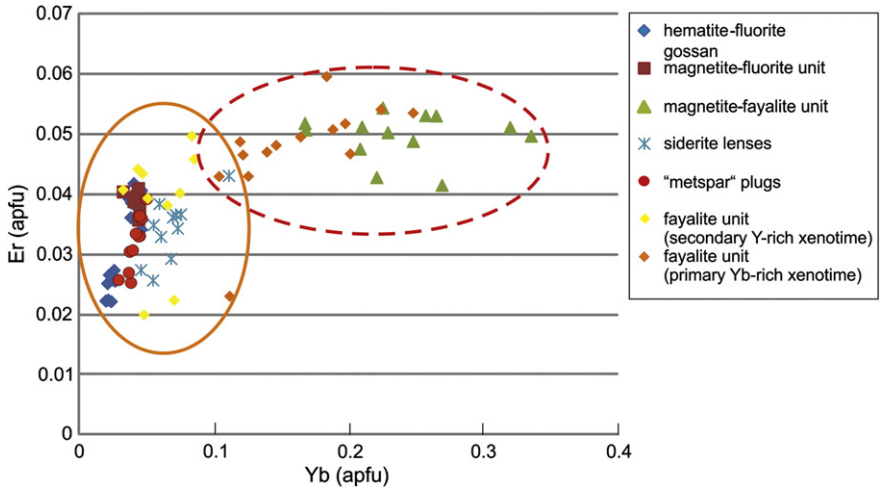

Fig. 6. Erbium vs. Yb plot in atoms per formula unit (apfu) calculated to four atoms of oxygen, illustrating the compositional variation of REE in xenotime from different units of the Vergenoeg Complex. Orange outlined field: secondary and overprinted xenotime; field outlined by a red dashed line: primary xenotime.

uniform Nb_2O_5 (45–50 wt.%) and lower FeO (5–11.5 wt.%) values. Inclusions of Nb-rich Fe^{3+}-dominated oxides also occur in the samarskite. Significant concentrations of UO_2, WO_3 (occasionally), Y_2O_3, REE_2O_3 and minor levels of PbO_2, TiO_2, ThO_2 and SiO_2 were determined for individual samarskite grains (Table 3). The concentrations of these oxides also vary between the dark and bright zones. Tantalum was not observed in this mineral.

4.2.3.4.2. Fergusonite-(Y). Fergusonite-(Y) is rather common in all samples from the magnetite–fayalite unit; it generally occurs within more or less strongly altered rims around fayalite grain fragments. Additionally, small grains (~10 μm in size) enclosed in pyrosmalite-(Fe) were observed in a sample from the fayalite unit. Fergusonite is commonly closely intergrown with ferberite (atomic Fe/Mn ratio = 24.9) and martitized fine-grained magnetite II (Fig. 10e). The distribution and mineral association of the fergusonite suggest that its formation was related to hydrothermal overprinting of the magnetite–fayalite and fayalite units.

Fergusonite grains in the magnetite–fayalite unit are euhedral, ~10–40 μm in size and commonly zoned (Fig. 10e–f). The cores of zoned fergusonite grains (bright in BSE images) are enriched in Yb, whereas the darker (commonly outer) zones show increased contents of Fe and higher Y/Yb ratios. Some fergusonite grains show clear evidence of a later overgrowth by a dark fergusonite rich in Fe and some REE (Nd, Sm, Gd), but rather poor in Yb (Fig. 10f). Chondrite-normalized REE distribution patterns typical of the two compositional types of fergusonite are shown in Fig. 12. The first type illustrated by red lines has high concentrations of the LREE and some of the MREE (Gd–Dy) and is typical of dark (in BSE images) outer zones of zoned grains, whereas the black patterns, which are typical of the cores of zoned grains or of homogeneous fergusonite grains of the second type (both appearing bright in BSE), show enrichment in the heaviest REE (Yb, Lu; Table 3).

Furthermore, significant concentrations of UO_2 (especially in the dark zones; up to ~5 wt.%), WO_3 (occasionally; sometimes >10 wt.%) and minor Pb, Ti, Th and Si contents were measured in most of the grains. Tantalum was not observed in the fergusonite using WDX scanning for Ta Lα.

4.3. Rb–Sr and Sm–Nd isotope systematics of fluorite

The results of the Rb–Sr and Sm–Nd isotope analyses for fluorite separates from the different lithological units of the Vergenoeg pipe are compiled in Table 4. Duplicate analyses were performed for Sm–Nd in order to detect inhomogeneities within the separates due to either the presence of different fluorite generations or inclusions of REE-rich minerals (see above). These types of intergrowth/impurities could not be eliminated by hand picking. Initial $^{87}Sr/^{86}Sr$ and ε_{Nd} values were calculated for an age of 2054 Ma corresponding to the ages of the Lebowa Granite Suite and genetically likely related intrusive and rhyolites (Dorland et al., 2006; Harmer and Armstrong, 2000; Scoates et al., 2012; Walraven and Hattingh, 1993).

The Sm–Nd concentration and isotope data indicate within-sample heterogeneity. Whereas two samples (Ver 12-3.F/a, b; and SA 09-114.F/a, b) yield results identical within error for the two splits analyzed, the other samples show appreciable differences in the data for the two splits (Table 4). Compared to the rather uniform LREE to MREE pattern of the fluorites (see above), the differences in Sm/Nd revealed by the isotope analysis for two splits of individual samples or between different samples imply the presence of minerals either strongly enriched in LREE or HREE, which affect the Sm–Nd budget of the separates even at very low modal amounts of these impurities.

5. Discussion

5.1. Constraints on the origin of the mineralization at Vergenoeg

Geologic field evidence (e.g., distribution of the main fluorite mineralization in the pipe rocks) and microscopic observations (e.g., crystal habits of fluorite, CL data) point to a magmatic origin of the economic fluorite mineralization at Vergenoeg. Microscopic examinations also reveal that fluorite in individual samples was affected to various degrees by subsequent alteration.

According to their Sr concentrations (26–39 ppm) and initial $^{87}Sr/^{86}Sr$ values (ca. 0.7154–0.7286), the analyzed fluorites correspond to "primary magmatic" fluorites of Kinnaird et al. (2004). The measured Sr concentrations and isotopic values are within the range of fluorite data reported by these authors and by Goff et al. (2004) for the Vergenoeg mine. In an Rb–Sr isochron plot (not shown), the data points strongly scatter without any obvious relation between $^{87}Sr/^{86}Sr$ and $^{87}Rb/^{86}Sr$. In this respect, the new Rb–Sr isotope results also match those of Goff et al. (2004) and Kinnaird et al. (2004) for the Vergenoeg fluorite. The interpretation of these authors that the uncorrelated $^{87}Sr/^{86}Sr$ and $^{87}Rb/^{86}Sr$ values most likely result from substantial secondary hydrothermal alteration is in line with the geochemical behavior of these hydrophile elements. Evidence for severe post-magmatic alteration of isotope systematics is also found in parts of the Lebowa Granite Suite (Hill et al., 1996; McNaughton et al., 1993) and in the volcanics of the Rooiberg Group (Buchanan et al., 2004).

According to their elevated Nd concentrations (56–157 ppm), the investigated fluorites correspond to the group of "high-Nd primary magmatic" fluorites from the Bushveld Complex (Kinnaird et al., 2004). In contrast to the Rb–Sr isotope system, the variation in the

Please cite this article as: Graupner, T., et al., Mineralogy of high-field-strength elements (Y, Nb, REE) in the world-class Vergenoeg fluorite deposit, South Africa, Ore Geol. Rev. (2014), http://dx.doi.org/10.1016/j.oregeorev.2014.02.012

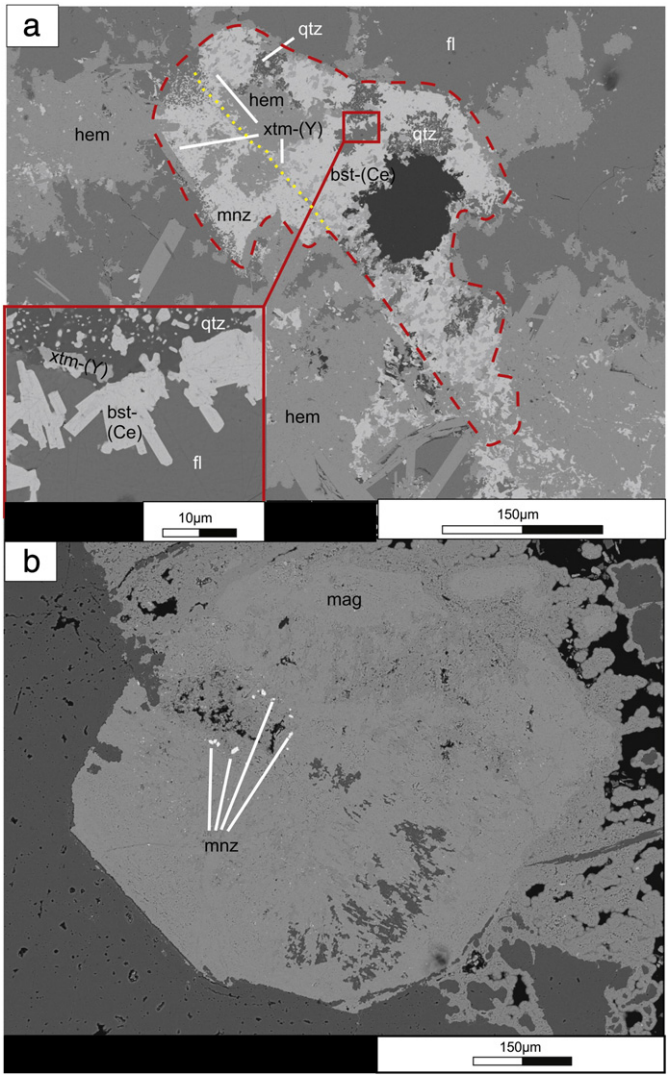

Fig. 7. BSE images of partly to completely replaced primary minerals in the Vergenoeg rocks. (a) Pseudomorph after fayalite in the hematite–fluorite gossan: areas dominated by monazite-(Ce) and bastnäsite-(Ce) are separated by a yellow dotted line. The pseudomorph also hosts small aggregates (mostly < 10 µm) of xenotime. (b) Sample from magnetite–fluorite unit containing early euhedral magnetite grains with finger-like areas of replacement highlighted by small monazite aggregates; the magnetite is replaced by various Fe oxyhydroxides. Abbr.: bst-(Ce): bastnäsite-(Ce); other symbols as in Figs. 2 and 5.

Sm–Nd data within individual samples and between samples can be related to processes, experienced by the Vergenoeg fluorite during its formation or very soon afterwards. This is obvious from a plot of $^{147}Sm/^{144}Nd$ versus $^{143}Nd/^{144}Nd$ (Fig. 13), where the data points of all samples form a well defined isochron corresponding to an age of 2040 ± 46 Ma (MSWD 0.34). Thus, our data do not confirm the results of Sm–Nd isotope investigations by Goff et al. (2004) and Kinnaird et al. (2004), which both indicate a considerable scatter of Sm–Nd isotope values among the Vergenoeg fluorite samples. The new Sm–Nd isochron age of 2040 ± 46 Ma represents the first direct age determination for fluorite mineralization within the Bushveld Complex. Within error, this age corresponds to more recent age determinations for different magmatic lithologies of the Bushveld Complex (e.g., Rajesh et al., 2013). A close temporal relation between fluorite mineralization and igneous processes within the Bushveld Complex is also supported by U–Pb ages of on average 2053 Ma for monazite from a fluorite-mineralized pegmatite associated with the Nebo Granite (Lebowa Granite Suite; Buick et al., 2011). Assuming an age of 2054 Ma, the fluorite separates provide a well defined initial $^{143}Nd/^{144}Nd$ of 0.509683 ± 0.000011 corresponding to an ε_{Nd} value of −5.6 ± 0.2. This value is significantly lower compared to the initial ε_{Nd} values reported by Kinnaird et al. (2004) for "primary magmatic" fluorites (ε_{Nd} +10.2 to −1.9) but within the range of initial ε_{Nd} values given by Goff et al. (2004) for fluorite from the Vergenoeg pipe (−4.2 to −6.9). The ε_{Nd} value of −5.6 is within error identical to the $^{143}Nd/^{144}Nd$ (t = 2054 Ma) values reported by Hill et al. (1996) for the Lebowa Granite Suite from the Dennilton region within the Bushveld Complex (ε_{Nd} −4.0 to −6.2). The volcanics of the Rooiberg Group, which, according to the dominantly evolved bulk-rock compositions compare to the Lebowa Granite Suite, show more evolved Nd isotope compositions (ε_{Nd} −6.6 to −10.2) (Buchanan et al., 2004). Genetic relation of the Rooiberg Group volcanics to the fluorite deposits is thus unlikely.

In a plot of Tb/Ca vs. Tb/La (both as atomic ratios) for fluorite from the Vergenoeg pipe (Fig. 14), both the ICP-MS and laser-ablation ICP-MS data for the economic fluorite mineralization (fluorite type I) from the major lithological units of the pipe cluster between the fields for pegmatitic and hydrothermal fluorite formation as defined by Möller et al. (1976) and Constantopoulos (1988). The new data correspond well to the data field for the "Vergenoeg fluorite sub-type of primary Lebowa Granite Suite-derived fluorite" of Crocker et al. (1988; field B in our Fig. 14). This field included REE data for primary fluorite from the Zwartkloof, Buffalo, Vergenoeg and Vellefontein mines. Interestingly, the data points for the "metspar" plug fluorites from this study are concentrated towards the upper end of a trend towards higher Tb/Ca and Tb/La ratios, delineated by the fluorite of type I from all major units of the Vergenoeg pipe (Fig. 14). This is indicative of higher level of REE fractionation in the "metspar" fluorite and suggests that this mineralization developed later than elsewhere (cf. Möller et al., 1976). The Vergenoeg field of Crocker et al. (1988) and our primary type I fluorite

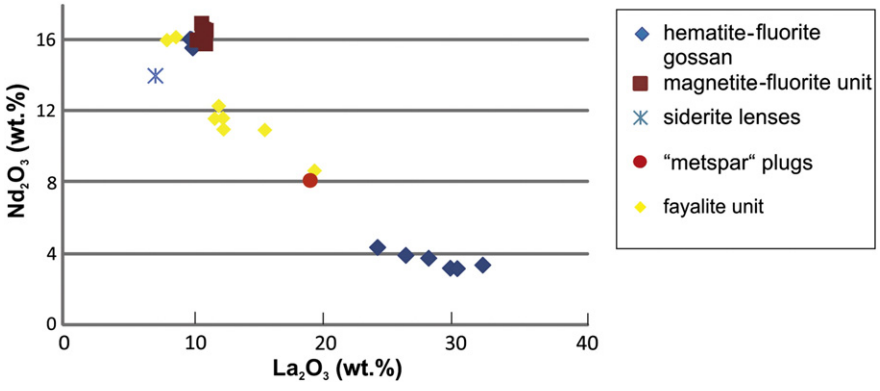

Fig. 8. Plot of Nd_2O_3 vs. La_2O_3 (in wt.%) for monazite from various lithological units of the Vergenoeg pipe.

Please cite this article as: Graupner, T., et al., Mineralogy of high-field-strength elements (Y, Nb, REE) in the world-class Vergenoeg fluorite deposit, South Africa, Ore Geol. Rev. (2014), http://dx.doi.org/10.1016/j.oregeorev.2014.02.012

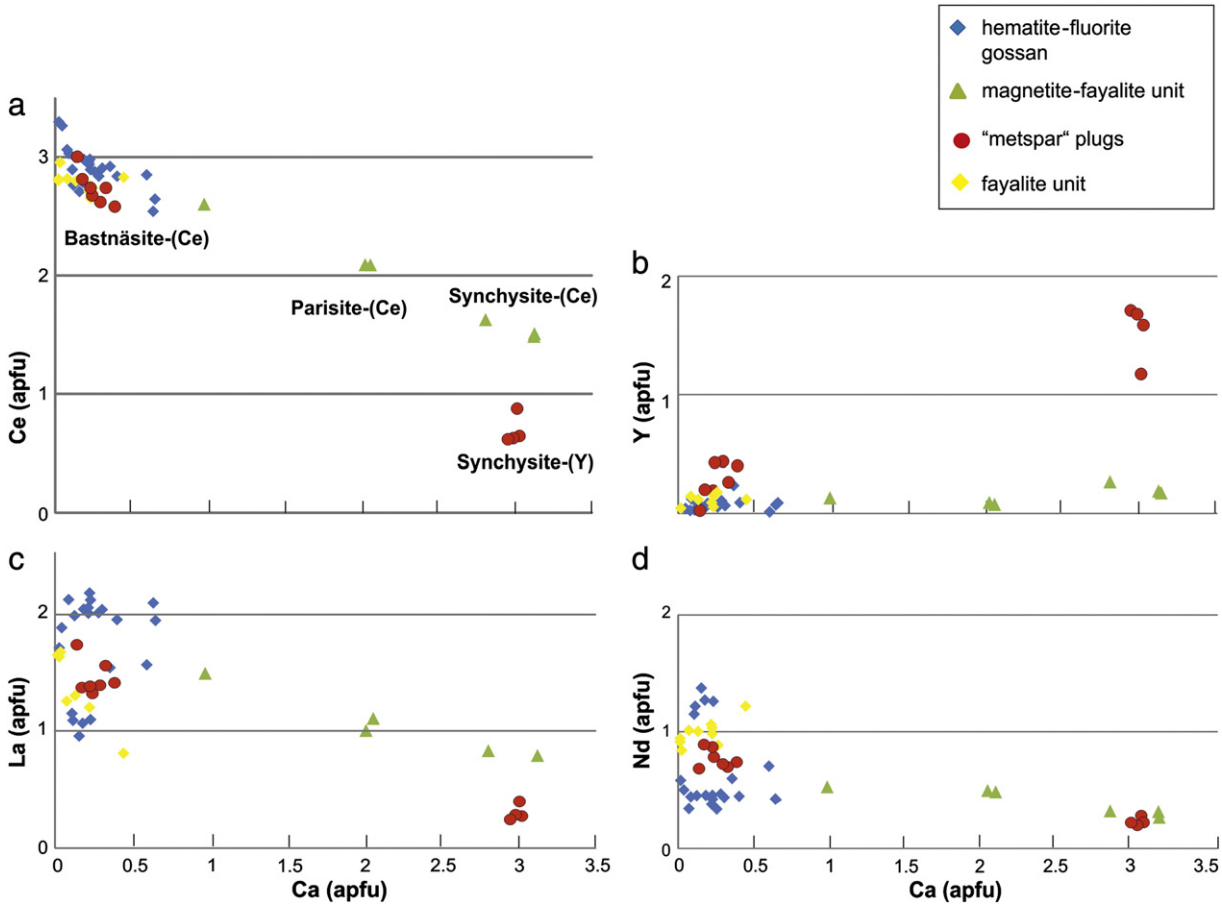

Fig. 9. Compositional variation of REE fluorocarbonates in the Vergenoeg deposit expressed as cation apfu values calculated from the EPMA results on the basis of a total of six cations (cf. Ruberti et al., 2008): (a) Ce vs. Ca; (b) Y vs. Ca; (c) La vs. Ca; (d) Nd vs. Ca.

data overlap significantly with the field for primary fluorite associated with cassiterite at Zaaiplaats (field A in Fig. 14).

However, data for the finer-grained fluorite aggregates of type II from the siderite lenses at Vergenoeg plot in the middle of the hydrothermal field in the Tb/Ca vs. Tb/La plot (Fig. 14), at lower Tb/Ca values than the type Ia fluorite. The compositions of the coarse-grained type Ib fluorite in the siderite lenses overlap with both of the above fields. These differences, interpreted in the context of the CL data, indicate that the siderite lenses represent zones of increased replacement of the early coarse-grained, REE-rich fluorite of type I by the finer-grained fluorite of type II with lower REE contents. Furthermore, all fluorite overgrowing late-stage REE minerals in cavities (or pseudomorphs) is clearly late hydrothermal in origin.

5.2. Distribution of the HFSE mineralization in the different lithological units of the pipe

All lithological units within the Vergenoeg pipe show strong enrichment in HFSE, including REE, Y and Nb (Fourie, 2000; Goff et al., 2004; this work). However, our work revealed that the distribution of HFSE appears to be heterogeneous within the pipe. The REE distribution patterns for whole-rock samples from the individual units show, despite a number of similarities, some striking differences among the units involving the relative proportion of LREE, MREE and HREE, or even individual lanthanoids (Fig. 15).

Firstly, the topmost portions of the pipe composed of the magnetite–fluorite unit and hematite–fluorite gossan resulting mainly from the weathering of the magnetite–fluorite unit, clearly host the highest TREO concentrations of all the units within the pipe. Even greater enrichment in REE is associated with the contact zone of the pipe at the rhyolitic carapace. The magnetite–fayalite and fayalite units have variable, but in most cases, much lower TREO concentrations. The plug-like "metspar" bodies are characterized by rather uniform TREO contents at intermediate concentrations (Fig. 15; Table 1).

Secondly, some of the pipe rock REE distribution patterns (Fig. 15) are, despite the obvious differences in the rock types, somewhat similar to concave-upward (or U-shaped) REE patterns of the Lease and Bobbejaankop Granites from the Zaaiplaats and Mutue Fides tin-mining regions (Hill et al., 1996). Unmineralized Nebo granites of the Lebowa Granite Suite and Rooiberg Felsites from the Enkeldoorn and Dennilton areas (S and E of Vergenoeg, respectively) have different patterns; they display a strong decrease in the chondrite-normalized values from LREE to HREE (Hill et al., 1996). The shapes of the patterns in the rhyolites at the contact with the Vergenoeg pipe (Fig. 15) are similar to those of the Nebo granites; however, the REE + Y concentrations are higher by three orders of magnitude in the rhyolites than in all of the granites.

The shape of the chondrite-normalized REE distribution patterns from the Vergenoeg pipe rocks shows two general types: (i) a more or less flat pattern from LREE to HREE (sometimes slightly decreasing values towards the heaviest REE), which is typical of magnetite–fluorite, hematite–fluorite, "metspar" and siderite lens samples, and (ii) a U-shaped REE pattern (with strong enrichment towards the heaviest REE), which characterizes the magnetite–fayalite and fayalite samples. To understand the differences in REE distribution patterns among the various rock units, a review of the HFSE mineralogy of these different pipe rocks is essential. A summary of all HFSE-enriched minerals identified in the present work is given in Table 5.

The available ICP-MS and laser-ablation ICP-MS data show that the fluorite of type Ia with invariable REE distribution patterns clearly

Please cite this article as: Graupner, T., et al., Mineralogy of high-field-strength elements (Y, Nb, REE) in the world-class Vergenoeg fluorite deposit, South Africa, Ore Geol. Rev. (2014), http://dx.doi.org/10.1016/j.oregeorev.2014.02.012

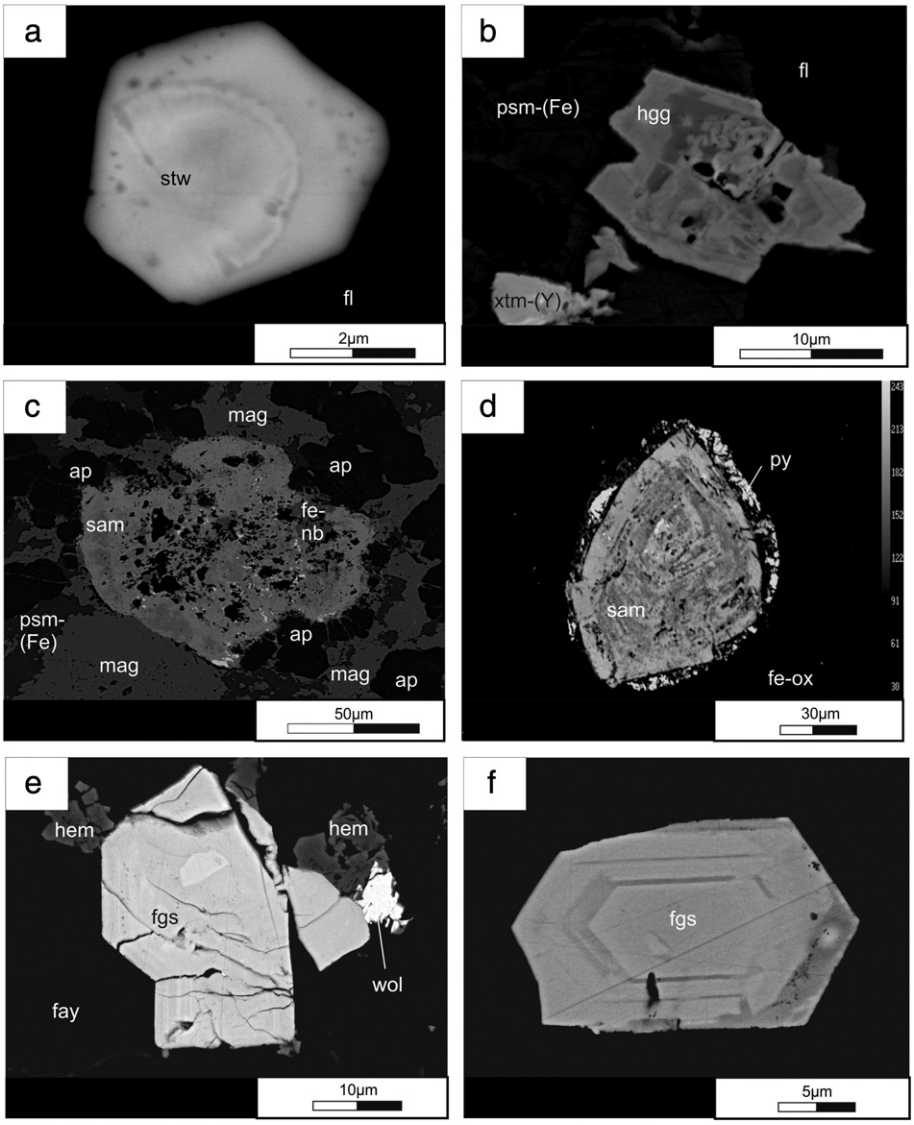

Fig. 10. BSE images of various REE silicates and oxides from Vergenoeg. (a) Hematite–fluorite gossan: euhedral stillwellite(?) grain enclosed in fluorite. (b) Fayalite unit: veinlet cross-cutting fluorite is filled with euhedral hingganite(?), Y-rich xenotime and pyrosmalite-(Fe). (c) Magnetite–fayalite unit: corroded samarskite grain associated with apatite and magnetite I. (d) Magnetite–fayalite unit: euhedral samarskite surrounded by a late pyrite rim. (e) Magnetite–fayalite unit: fergusonite intergrown with ferberite and martitized magnetite II. (f) Magnetite–fayalite unit: euhedral zoned fergusonite. Abbr.: ap: apatite; fay: fayalite; fgs: fergusonite; hgg: hingganite; fe-nb: iron oxide-(Nb-bearing); sam: samarskite; stw: stillwellite; wol: ferberite; other symbols as in Figs. 2, 5 and 7.

predominates in most of the units throughout the Vergenoeg pipe (Fig. 3; Table 2). The only exceptions are the siderite lenses, where two fluorite types can be distinguished. Secondly, significant amounts of apatite are present in samples from deeper parts of the pipe only (Borrok et al., 1998; this study). Consequently, fluorite and apatite cannot be responsible for the observed differences in REE distribution patterns among the units.

Fig. 16 illustrates the strong influence of the REE phosphate minerals on the distribution of REE in the Vergenoeg pipe. The P_2O_5 vs. total REE + Y diagram shows that most of the samples plot on a trend formed by the major lithological units; however, there also appears to be another trend parallel to this main trend. This second trend is formed by the "metspar" samples and REE-enriched rhyolite from the marginal zone of the pipe. The second trend with significantly higher REE values at similar P_2O_5 concentrations indicates that REE minerals other than phosphates predominate in the "metspar" plugs and the rhyolite.

The most common REE mineral throughout the Vergenoeg pipe is xenotime (Table 5) occurring as two chemical varieties, Yb-rich and Y-rich xenotime. The early, Yb-rich xenotime is very common, but restricted to the magnetite–fayalite and fayalite units (Table 5). The later-crystallized, MREE-Y-rich xenotime is very common in the hematite–fluorite and magnetite–fluorite units and is locally present in the other rocks. The only other minerals at Vergenoeg that significantly concentrate MREE and HREE, are the niobium-rich oxides samarskite and fergusonite. Again, these latter minerals are only present in the magnetite–fayalite and fayalite units (Table 5). Consequently, the significant differences between the two general types of chondrite-normalized REE distribution pattern at Vergenoeg (see Fig. 15 and preceding discussion) are caused by the distribution of (i) the compositionally different xenotime and (ii) the Nb-rich REE-bearing oxide minerals.

Monazite-(Ce) is common in the hematite–fluorite gossan and magnetite–fluorite unit; however, it occurs only in subordinate amounts in other rock types. Bastnäsite-(Ce) and the other, much less common, REE fluorocarbonates occur throughout the pipe. The common occurrence of bastnäsite-(Ce) in the gossan, "metspar" plugs and especially at the pipe margin is responsible for the LREE- to MREE-dominated chondrite-normalized patterns of these rocks (Fig. 15). Rare earth-bearing silicates are too scarce in all lithological units at Vergenoeg to

Please cite this article as: Graupner, T., et al., Mineralogy of high-field-strength elements (Y, Nb, REE) in the world-class Vergenoeg fluorite deposit, South Africa, Ore Geol. Rev. (2014), http://dx.doi.org/10.1016/j.oregeorev.2014.02.012

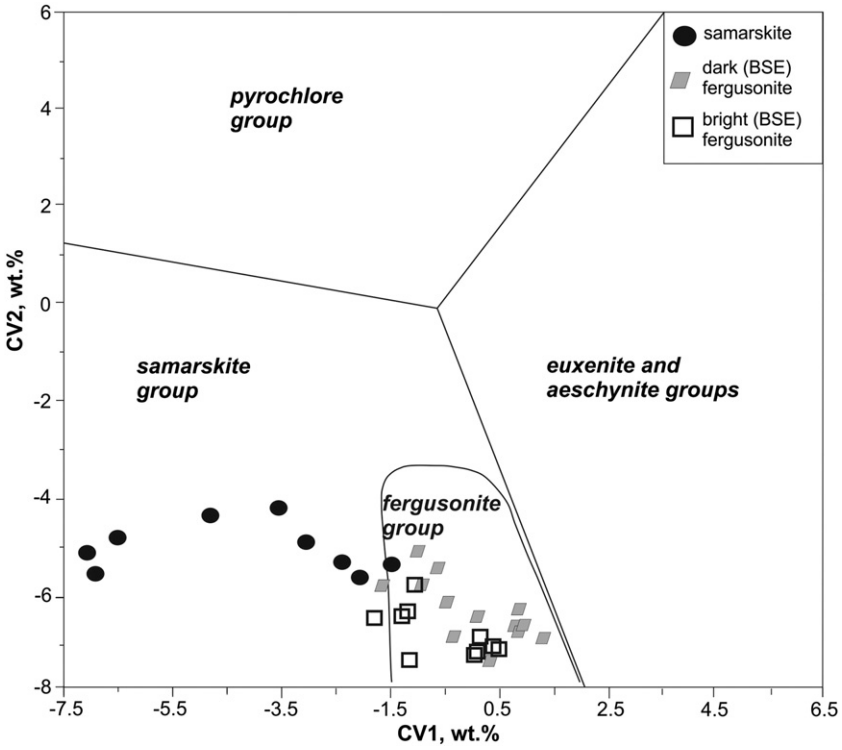

Fig. 11. The composition of HFSE oxides from Vergenoeg plotted in the empirical diagram of Ercit (2005) used to discriminate among complex (Y,REE,U,Th)–(Nb, Ta,Ti) oxide minerals (for further details of this method, see Ercit, 2005).

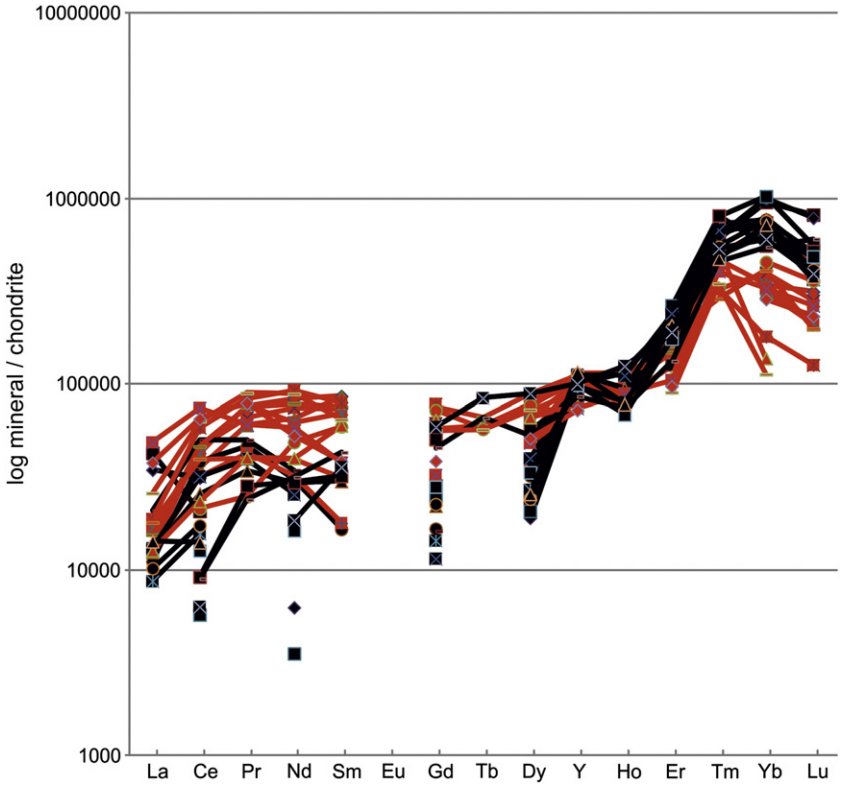

Fig. 12. Chondrite-normalized REE–Y distribution patterns for different types of fergusonite from the Vergenoeg pipe. Red lines stand for heavy REE (Yb, Lu)-poor and light and middle REE (e.g. Nd)-rich; black lines stand for heavy REE-rich and light to middle REE-depleted fergusonite. The data are chondrite-normalized using the values of McDonough and Sun (1995). Note that some of the elements are below their detection limit in some or all (Eu) of the samples.

Please cite this article as: Graupner, T., et al., Mineralogy of high-field-strength elements (Y, Nb, REE) in the world-class Vergenoeg fluorite deposit, South Africa, Ore Geol. Rev. (2014), http://dx.doi.org/10.1016/j.oregeorev.2014.02.012

Table 4
Rb–Sr and Sm–Nd isotope data for fluorite separates from the Vergenoeg mine. Samples were analyzed for Sm–Nd in duplicate.

Sample	Split	Lithological unit	Rb (ppm)	Sr (ppm)	$^{87}Rb/^{86}Sr$	$^{87}Sr/^{86}Sr$ (measured)	$(^{87}Sr/^{86}Sr)_i$[a]	Sm (ppm)	Nd (ppm)	$^{147}Sm/^{144}Nd$	$^{143}Nd/^{144}Nd$ (measured)	ε_{Nd}[b] (pr.d.)[c]	ε_{Ndi}[a]
SA 09-103.F	a	Hematite–fluorite (gossan)	0.16	34.20	0.0135	0.720938	**0.72054**	36.68	122.99	0.1803	0.512123	−10.0	**−5.7**
	b							42.15	156.63	0.1627	0.511888	−14.6	**−5.7**
SA 09-106.F	a	Hematite–fluorite (gossan)	0.67	36.33	0.0531	0.723668	**0.72210**	29.17	95.36	0.1849	0.512192	−8.7	**−5.6**
	b							25.68	85.70	0.1811	0.512142	−9.7	**−5.6**
SA 09-111.F	a	Siderite lens	0.47	26.13	0.0521	0.726351	**0.72481**	31.69	115.27	0.1662	0.511950	−13.4	**−5.4**
	b							32.21	122.89	0.1584	0.511844	−15.5	**−5.5**
SA 09-114.F	a	Magnetite–fayalite	0.17	27.68	0.0175	0.716346	**0.71583**	15.68	55.93	0.1695	0.511988	−12.7	**−5.6**
	b							15.70	55.97	0.1695	0.511980	−12.8	**−5.7**
SA 09-119.F	a	"Metspar" lens	0.35	33.99	0.0295	0.716269	**0.71540**	43.81	131.83	0.2009	0.512412	−4.4	**−5.5**
	b							44.81	133.57	0.2028	0.512436	−3.9	**−5.5**
SA 09-123.F	a	Fayalite	0.30	35.28	0.0243	0.720276	**0.71956**	24.09	70.74	0.2059	0.512476	−3.2	**−5.6**
	b							26.58	79.54	0.2020	0.512421	−4.2	**−5.6**
Ver 12-3b.F	a	Magnetite–fluorite	0.27	39.00	0.0201	0.729145	**0.72855**	27.68	94.29	0.1775	0.512092	−10.7	**−5.6**
	b							27.61	94.02	0.1776	0.512097	−10.6	**−5.5**

[a] Initial $^{87}Sr/^{86}Sr$ and ε_{Nd} values (in bold) were calculated for an age of 2054 Ma.
[b] ε_{Nd} values are based on $^{147}Sm/^{144}Nd = 0.1967$ and $^{143}Nd/^{144}Nd = 0.512638$ for CHUR ("chondritic uniform reservoir", Jacobsen and Wasserburg, 1980).
[c] pr.d. denotes present-day values.

contribute to the REE budget of their host rocks to any significant degree.

Niobium-rich minerals occur restricted to the magnetite–fayalite and fayalite units. Here, samarskite and fergusonite are rather common in most of the samples. All other units of the pipe seem to be devoid of discrete Nb-rich mineral phases. However, the bulk rock analytical data for the pipe rocks show evidence of Nb fractionation as a consequence of weathering (Table 1). In the topmost units of the pipe (magnetite–fluorite unit and gossan), the Nb concentrations reach maximum values, compared to moderate Nb values in the fayalite and magnetite–fayalite rocks, and low Nb values (<10 ppm) in all other rock types. Element mapping of gossan samples using SEM with EDX indicated that fine-grained Fe-rich alteration products probably host the elevated Nb concentrations. This observation is in agreement with the data of Wall et al. (1996), who described Nb-bearing goethite from laterite overlying pyrochlore-rich carbonatite at Lueshe, Democratic Republic of Congo. On the other hand, Škoda et al. (2011) found heterogeneous Nb-rich mixtures of nano-scale, possibly amorphous hydrated oxides, phosphate-arsenates, as well as silicates of U, Fe and Ca formed as a result of alteration of Y–REE–Nb–Ta–Ti-oxide minerals from Obrazek pegmatite, Czech Republic.

Tantalum concentrations show no clear trend when the individual lithological units are compared and are too low to be measured in individual mineral grains using EPMA.

5.3. Constraints on the formation of the magmatic enrichment and later redistribution of HFSE at Vergenoeg

Our petrographic and geochemical observations indicate that the HFSE minerals in the Vergenoeg pipe rocks have formed during several consecutive stages. Significant remobilization of HFSE from earlier-developed mineralization (partly preserved in lower parts of the pipe; see below) and their subsequent redistribution into the near-surface gossan and adjacent wall-rock contacts are inferred. Interaction of

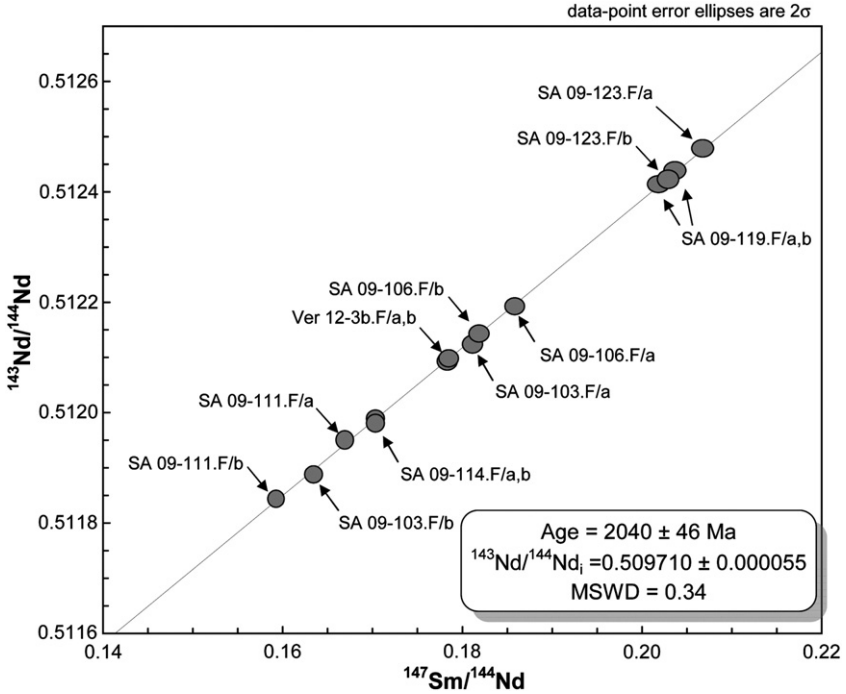

Fig. 13. Sm–Nd isochron diagram for fluorite separates analyzed in duplicate splits from the Vergenoeg mine. See text for details.

Please cite this article as: Graupner, T., et al., Mineralogy of high-field-strength elements (Y, Nb, REE) in the world-class Vergenoeg fluorite deposit, South Africa, Ore Geol. Rev. (2014), http://dx.doi.org/10.1016/j.oregeorev.2014.02.012

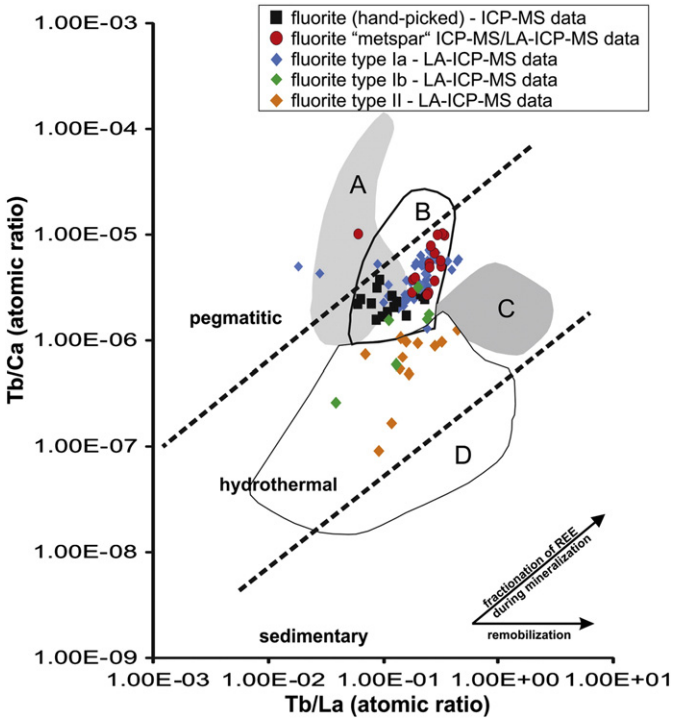

Fig. 14. Plot of Tb/Ca vs. Tb/La (atomic ratios) for fluorite from the Vergenoeg pipe (ICP-MS and LA–ICP-MS data). For more details on fluorite types Ia, Ib and II, see Subsection 4.2.1. Fields A to D are from Crocker et al. (1988) and stand for: A–C — primary granite-derived fluorite in granites, pipes and stockworks (A — Zaaiplaats fluorite subtype, B — Vergenoeg fluorite subtype, C — Blockspruit fluorite subtype), and D — secondary fluorite, epithermal fillings in veins, open fissures and cavities from all locations containing subtypes A–C.

REE-bearing hydrothermal fluids and the wall-rocks could have triggered the precipitation of significant volumes of REE minerals (Giere, 1996).

However, significant addition of mineralized fluids (HFSE-bearing) from external sources can be ruled out (cf. Kinnaird et al., 2004) based on the limited variation of Sr concentrations and initial $^{87}Sr/^{86}Sr$ values of fluorite throughout the pipe. Schütte (2005) infers that the Vergenoeg pipe magma itself may constitute the source of the REE in the system. This conclusion is based on the data of Watson (1976), which indicate strong partitioning of REE into immiscible Fe-rich liquids that probably produced the Vergenoeg pipe rocks. Evidence for an autometasomatic overprint of these rocks includes the disturbed Rb–Sr isotope signature of the Vergenoeg fluorite. Fluorite separates from the different units of the pipe yield a well-defined Sm–Nd isochron age of 2040 Ma and a very homogeneous initial Nd isotope composition corresponding to an ε_{Nd} of −5.6. Bearing in mind that these fluorite samples likely contain minor impurities of high-REE minerals, which may significantly contribute to the Sm–Nd budget of the separates, this isotopic uniformity strongly suggests a unique homogenous source of the REE not only in fluorite from the different units, but also in the associated high-REE accessory minerals. Evidence for a "foreign" REE component, introduced for instance by metasomatic or secondary processes capable of modifying the Sm–Nd isotope systematic, is missing. Based on the close similarities between the fluorite isochron age and the age data for magmatic rocks of the Bushveld Complex on the one hand, and between the initial Nd isotope compositions of the Vergenoeg pipe and of some of the Lebowa granites on the other hand, we conclude that the REE budget of the pipe was directly derived from a Lebowa-type granitic magma, and that the pipe and its associated fluorite mineralization formed within the same time frame as the other magmatic rock units of the Bushveld Complex. As noted in other studies of magmatic rocks from the Bushveld Complex, there is, however, evidence for secondary hydrothermal alteration of the Vergenoeg pipe rocks. This process led to redistribution of hydrophile elements (for instance Rb and Sr) and may be responsible for the differences in Sr concentration observed in type Ia, Ib and II fluorite (Table 2).

The identification of primary HFSE-rich mineral phases in the strongly weathered gossan is not possible. Early-stage HFSE minerals are mainly preserved in the magnetite–fayalite and fayalite units. Textural relationships, like their intergrowth with early coarse-grained magnetite I and apatite, indicate that the coarse-grained, zoned and marginally corroded grains of Nb-rich samarskite formed during the primary, magmatic stage.

Higher-temperature hydrothermal precipitation of euhedral, zoned fergusonite is inferred based on its common paragenetic association with ferberite and fine-grained magnetite II (later martitized; Fig. 10e). The Fe-dominant composition of the Vergenoeg wolframite reflects the high levels of Fe and low levels of Mn in the studied rocks and provides no additional constraints on the temperature of its crystallization (Wood and Samson, 2000). Fergusonite occurs along altered grain boundaries of coarse-grained and partly replaced magmatic fayalite

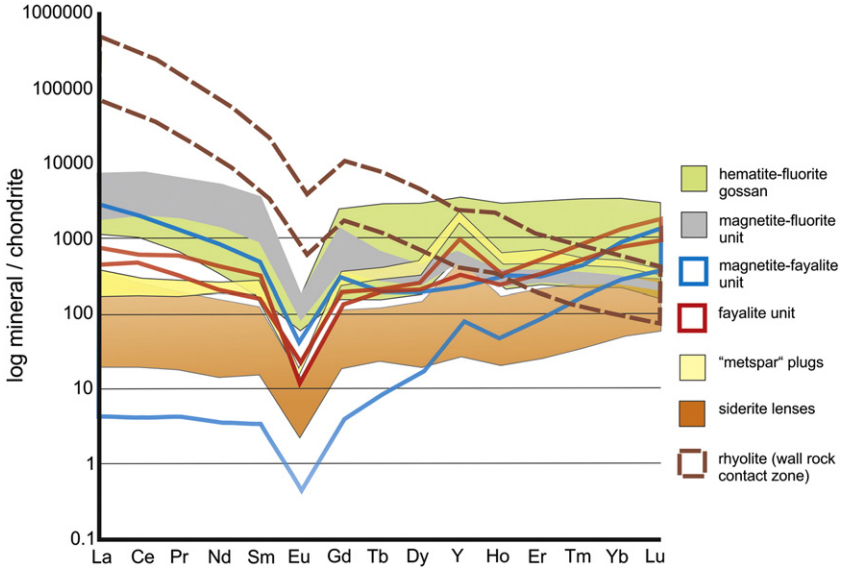

Fig. 15. Chondrite-normalized REE–Y distribution patterns for whole-rock samples from major lithological units, as well as from siderite lenses and "metspar" plugs from the Vergenoeg pipe. All data are chondrite-normalized using the values of McDonough and Sun (1995).

Please cite this article as: Graupner, T., et al., Mineralogy of high-field-strength elements (Y, Nb, REE) in the world-class Vergenoeg fluorite deposit, South Africa, Ore Geol. Rev. (2014), http://dx.doi.org/10.1016/j.oregeorev.2014.02.012

Table 5
Summary of REE minerals found in the igneous Vergenoeg deposit, South Africa.

Rock unit-Sample	REE mineral phases	Association	Abundance
Hematite–fluorite gossan	Y-rich xenotime	In Fe oxides, fluorite; with REE fluorocarbonates, monazite, sulfates, quartz	Very common
	Monazite-(Ce)	In hematite; with Y-rich xenotime, REE fluorocarbonates, quartz	Common
	Monazite-(La)	In hematite; with fine-grained fluorite	Locally common
	Bastnäsite-(Ce)	In hematite and fluorite; with Y-rich xenotime, monazite, quartz	Common
	Stillwellite(?)	In fluorite	Rare
Magnetite–fluorite unit	Y-rich xenotime	In Fe oxide and fluorite; with monazite	Very common
	Monazite-(Ce)	In Fe oxyhydroxides and fluorite; with Y-rich xenotime	Very common
	Bastnäsite-(Ce)	In Fe-oxide and pyrosmalite-(Fe)(?)	Locally present
"Metspar" plugs	Y-rich xenotime	In veinlets and as inclusions in fluorite; with Fe oxide, monazite, pyrite, chalcopyrite, chalcocite, REE fluorocarbonate	Common
	Monazite-(Ce)	In fluorite; with Y-rich xenotime	Very rare
	Synchysite-(Y)	In fluorite	Rare
	Bastnäsite-(Ce)	In veinlets cross-cutting fluorite; quartz, pyrite, Y-rich xenotime, chalcopyrite	Common
	Fluocerite-(Ce)	In veinlet cross-cutting fluorite and in cavities; with Fe oxide, Y-rich xenotime	Rare
	Okanoganite(?)	In veinlet in fluorite; with pyrite and chalcopyrite	Very rare
	Hingganite-(Y)(?)	In cavities in fluorite	Very rare
Siderite lenses	Y-rich xenotime	In siderite; with sulfides, monazite	Rare
	Monazite-(Ce)	In siderite; with pyrite, Y-rich xenotime	Rare
Magnetite–fayalite unit	Apatite	With magnetite I, samarskite, pyrosmalite-(Fe), parisite-(Ce)	Locally very common
	Yb-rich xenotime	In greenalite, pyrosmalite-(Fe), altered fayalite	Very common
	Synchysite-(Ce)	With magnetite I, pyrosmalite-(Fe), fluorite	Locally common
	Parisite-(Ce)	In altered apatite-magnetite I aggregates; with pyrosmalite-(Fe)	Locally common
	Bastnäsite-(Ce)	Forms thin overgrowth on synchysite-(Ce)	Locally common
	Hingganite-(Y)(?)	In fayalite	Very rare
	Samarskite-(Y)	With magnetite I, apatite, pyrosmalite-(Fe), Fe oxides, pyrite	Locally common
	Fergusonite-(Y)	In altered fayalite, pyrosmalite-(Fe); with magnetite II (martitized), ferberite	Common
Fayalite unit	Yb-rich xenotime	In greenalite, pyrosmalite-(Fe)/altered fayalite; with quartz	Very common
	Y-rich xenotime	In Fe oxides and in veinlets cross-cutting fluorite; with monazite, siderite, sulfides	Locally common
	Monazite-(Ce)	In pyrosmalite-(Fe)/fayalite; with Fe oxides, Y-rich xenotime, pyrite, quartz, U mineral, siderite	Common
	Bastnäsite-(Ce)	In fluorite and altered fayalite; with Fe oxides, pyrite, arsenopyrite	Rare
	Hingganite-(Y)(?)	In veinlet with pyrosmalite-(Fe) and Y-rich xenotime	Very rare
	Fergusonite-(Y)	In pyrosmalite-(Fe)	Rare

and should, consequently, be somewhat younger than the fayalite. The grains of fine-grained magnetite II probably formed at the expense of fayalite.

According to Borrok et al. (1998), allanite represents the most common REE-rich mineral in the primary assemblage at Vergenoeg (about 2% of the primary assemblage). However, no allanite was observed in this study. Pseudomorphs are common in samples from the near-surface areas of the Vergenoeg pipe; however, they are present in all other major lithological units, as well. The preserved crystal shapes of the replaced minerals and the presence of Si- and Fe-rich secondary phases indicate fayalite as the most common precursor mineral. However, the magnetite–fayalite unit also contains blade-like pseudomorphs filled with closely intergrown needle-like and extremely fine-grained chlorite(?), Fe oxides and various REE minerals (including bastnäsite). This assemblage may result from interaction of early allanite with a fluid and its transformation into secondary minerals (cf. Giere, 1996).

No xenotime was found enclosed in fayalite, magnetite I or other magmatic minerals, making early magmatic formation of this mineral highly unlikely. Coarse-grained, subhedral to euhedral grains of Yb-rich xenotime occur randomly distributed in greenalite or its decay products (Fig. 5a,b) within the magnetite–fayalite and fayalite lithological units.

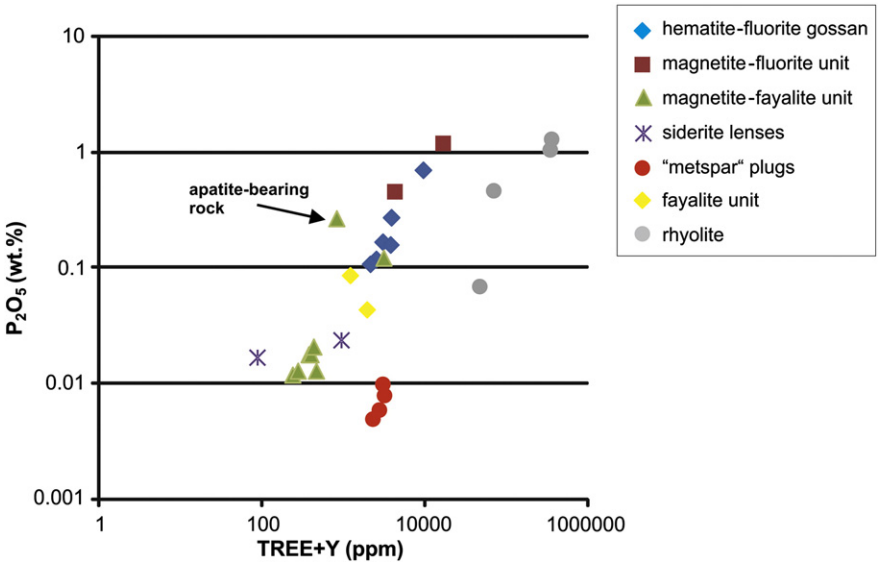

Fig. 16. Plot of P_2O_5 (wt.%) vs. total REE + Y content (ppm) in lithological units of the Vergenoeg pipe and in rhyolite from the pipe margin (ICP-MS data).

Please cite this article as: Graupner, T., et al., Mineralogy of high-field-strength elements (Y, Nb, REE) in the world-class Vergenoeg fluorite deposit, South Africa, Ore Geol. Rev. (2014), http://dx.doi.org/10.1016/j.oregeorev.2014.02.012

Consequently, these grains are interpreted to have precipitated during hydrothermal alteration of the Vergenoeg rocks and replacement of fayalite by greenalite (temperature conditions: max. ~300 °C, for H_2O-saturated FeO–SiO_2–H_2O system at 1 kbar; cf. Rasmussen et al., 1998). Aggregates of several coarse Yb-rich xenotime grains are scarce. It should be noted at this point that the early REE phosphates are less abundant in comparison with the very common late-stage REE phosphates. Probably, most of the phosphorus present in the rock-forming melt forming the pipe rocks was sequestered by the early apatite and, thus, not available during the early hydrothermal activity. The near-surface units containing the highest phosphate contents (Table 1; Fig. 16) were intensely overprinted by weathering, and the early phosphate-bearing HFSE minerals were completely destroyed in all studied samples, if ever present. Xenotime grains composed of an Yb-rich core and a Y-enriched secondary rim (Fig. 5c) were observed in greenalite(?) aggregates, replaced to a large extent by younger pyrosmalite-(Fe), from the fayalite unit; see below for discussion of the formation conditions of the late Y-rich xenotime.

Since there is no evidence for any significant contribution of mineralized fluids from external sources bearing complexed HFSE, alternative sources for the late enrichment of mostly LREE- and Y-bearing REE fluorocarbonates and phosphates in the near-surface regions of the pipe need to be discussed. Early HFSE-enriched minerals present in significant quantities in the pipe rock could have been apatite, fluorite Ia or allanite, as indicated by the petrographic data presented in this study, Borrok et al. (1998) and Goff et al. (2004). The mechanism and conditions of metasomatic alteration of REE–Y-bearing natural fluorapatite were studied by several authors. They found (i) depletion of the altered apatite in REE and (ii) concomitant nucleation of REE phosphates (monazite and xenotime) along grain boundaries of the altered apatite (e.g., Harlov and Förster, 2003). The loss of Si and/or Na from apatite during metasomatism results in charge imbalance and induces the release of REE + Y from the apatite structure. Torab and Lehmann (2007) studied the magnetite–apatite deposits of the Bafq district (central Iran) and observed nucleation of allanite, xenotime and parisite as a result of intense hydrothermal alteration of apatite and REE leaching. Harlov et al. (2002) suggested that leaching of Na, Si and LREE from apatite grains of magnetite–apatite ore from the Kiruna area (northern Sweden) took place initially under high-temperature conditions (700–800 °C) and then at lower temperatures, corresponding to the greenschist facies (300–450 °C). The dominating salt component in the related fluids could not have been NaCl as this would have stabilized Na and REE in the apatite via the coupled substitution $Na^+ + (Y + REE)^{3+} = 2Ca^{2+}$ (Harlov et al., 2002). Leaching of REE from fluorapatite and concomitant formation of parisite is well documented for Vergenoeg rocks in the present study (Fig. 4). Fluid-inclusion data of Borrok et al. (1998) show common Fe chloride daughter minerals in moderate- to high-temperature fluid inclusions in the Vergenoeg rocks, suggesting a significant role of Fe chloride in the fluid besides NaCl.

A partial or complete breakdown of the early apatite in the fayalite-bearing zones at Vergenoeg released significant Ca, P, F, Si, Cl, LREE and Y into the circulating hydrothermal fluid. This fits very well with our mineralogical observations, which indicate the development of rims, veinlets and cavity fillings of fluorite together with LREE minerals (fluorocarbonates, monazite), Y-rich xenotime, secondary fine-grained apatite and Cl-bearing pyrosmalite-(Fe). A late-stage origin of the widespread pyrosmalite-(Fe) veinlets in the Vergenoeg pipe rocks is consistent with the conclusion of Pan et al. (1993) that most pyrosmalite worldwide (e.g., Precambrian Geco, Willroy and Thomson mines, Canada) has a hydrothermal origin.

Abundant formation of low-temperature fine-grained REE phosphates (monazite-(Ce) and Y-rich xenotime) in the magnetite–fluorite unit and the gossan was probably caused by the elevated phosphate contents of these rocks (Fig. 16; cf. Harlov et al., 2002). Phosphate ions represent important REE-complexing agents (Giere, 1996) and, thus, may have prevented the REE from being flushed out of the rock.

Furthermore, late fine-grained REE minerals are often texturally closely associated with sulfides in the fayalite unit and "metspar" plugs (e.g., veinlet fillings; Fig. 5e). Here, changes in pH resulting from the conversion of metal chloride solutes to sulfide minerals might have induced deposition of the dissolved REE (Giere, 1996).

The distribution of the REE fluorocarbonates in the Vergenoeg pipe rocks as fillings in pseudomorphs, veinlets and fissures clearly indicates their late-stage formation. They are concentrated especially in the upper parts of the Vergenoeg pipe, including the gossan, "metspar" plugs and rhyolites at the pipe margin. The REE fluorocarbonates are interpreted to represent products of interaction of late fluorine-rich aqueous fluids causing local remobilization and re-deposition of REE (cf. Ngwenya, 1994). The occurrence of the bastnäsite–fluorite assemblage in the gossan (Fig. 7a) and in marginal rhyolite restricts the formation conditions of this assemblage to relatively low temperatures (<350 °C; Williams-Jones and Wood, 1992). The scarcity of synchysite in the "metspar" plugs, as well as the absence of calcite in all studied samples, constraints the formation of this REE fluorocarbonate assemblage to low pressures. This agrees well with the geological data that demonstrate that the Vergenoeg pipe formed in a subaerial environment. Coarse grains of synchysite-(Ce) exhibit a marginal overgrowth of bastnäsite-(Ce) and are restricted to the magnetite–fayalite unit, possibly indicating changes in the activities of Ca^{2+} or CO_3^{2-} in the circulating aqueous fluid (Giere, 1996).

Large-scale leaching and re-deposition by groundwater took place in the porous oxidized ores, particularly at the base of the gossan at Vergenoeg (e.g., Crocker et al., 1988). However, Ce anomalies were not observed in gossan rocks (bulk rock data) and were also not common in late, low-temperature HFSE minerals in this study. At present, it cannot be explained why Ce was not oxidized to Ce^{4+} (CeO_2) in the studied rocks.

6. Conclusions

1. Fluorite from different lithological units of the Vergenoeg pipe is largely magmatic in origin, with an age of 2040 ± 46 Ma and a very homogeneous initial Nd isotope composition (ε_{Nd} of −5.6 ± 0.2). Subsequent hydrothermal processes overprinted the primary textural and geochemical characteristics. Laser-ablation ICP-MS data indicate the presence of at least three distinct fluorite types (Ia, Ib and II).
2. Ore microscopy, SEM and EPMA reveal the presence of a wide variety of HFSE-bearing minerals in the Vergenoeg pipe. Niobium is hosted by either early-crystallized, complex oxide minerals of the samarskite and fergusonite groups, or Fe-rich alteration products in the gossan. Important carriers of REE + Y are xenotime, monazite-(Ce) and -(La) and bastnäsite-(Ce), with minor parisite-(Ce), synchysite-(Ce) and -(Y), fluocerite, hingganite, stillwellite and okanoganite (the latter three minerals were identified only tentatively owing to the lack of quantitative data for B and Be).
3. Two principal types of chondrite-normalized REE–Y distribution pattern are distinguished in the pipe rocks: (i) a more or less flat pattern typical of samples from the magnetite–fluorite and hematite–fluorite units, "metspar" plugs and siderite lenses, and (ii) a U-shaped pattern with strong enrichment towards the heaviest REE, characteristic of the magnetite–fayalite and fayalite units.
4. Xenotime represents an important carrier of MREE, HREE and Y throughout the Vergenoeg pipe. The distribution of its two compositional varieties, Yb-rich xenotime and Y-rich xenotime, largely controls the REE-Y distribution patterns summarized above. The Yb-rich xenotime is restricted to the fayalite-bearing units, whereas the Y-rich variety dominates in the rest of the lithological units.
5. The Sm–Nd isotope systematics of fluorite separates strongly suggest that the REE budget of the Vergenoeg pipe was derived from a Lebowa-type granitic magma. Isotopically, there is no evidence for any contribution from other REE sources. Formation of the pipe,

Please cite this article as: Graupner, T., et al., Mineralogy of high-field-strength elements (Y, Nb, REE) in the world-class Vergenoeg fluorite deposit, South Africa, Ore Geol. Rev. (2014), http://dx.doi.org/10.1016/j.oregeorev.2014.02.012

including the development of fluorite mineralization occurred within the same time frame as the emplacement of other magmatic rock units of the Bushveld Complex. Secondary hydrothermal processes are manifested in the strongly disturbed Rb–Sr isotope systematics.

6. HFSE mineralization in the Vergenoeg pipe rocks developed over several stages. Samarskite and coarse fluorapatite are part of the primary mineral assemblage. Fergusonite and Yb-rich xenotime formed during high- to moderate-temperature hydrothermal activity. Significant remobilization of the HFSE from the earlier mineralization (partial or complete breakdown of the fluorapatite and allanite(?) with release of REE and Y) and their subsequent redistribution into the near-surface gossan and adjacent wall-rock contacts are inferred. The late-crystallizing, low-temperature alteration assemblages are characterized by the presence of REE fluorocarbonates and phosphates (monazite and Y-rich xenotime).

Acknowledgments

The authors are grateful to the Vergenoeg Mining Company (Vergenoeg, Gauteng Province, South Africa), who allowed us to conduct investigations on their property. The technical assistance of J. Lodziak and C. Wöhrl (BGR Hannover) during microprobe work is appreciated. The authors express their gratitude to F. Korte (XRF lab), D. Weck (XRD lab), B. Harazim and H. Lorenz (both ICP-MS lab) as well as to S. Gerlach (TIMS lab) for their technical and analytical assistance at the BGR. Dr. H. Brätz (Erlangen-Nürnberg University) is thanked for the LA–ICP-MS work and Dr. H.-E. Gäbler is thanked for the discussion of LA–ICP-MS data. Three anonymous reviewers of Ore Geology Reviews and the handling guest editors Dr. J. Kynicky and Dr. A.R. Chakhmouradian provided useful comments which considerably improved the manuscript.

References

Borrok, D.M., Kesler, S.E., Boer, R.H., Essene, E.J., 1998. The Vergenoeg magnetite–fluorite deposit, South Africa; support for a hydrothermal model for massive Fe-oxide deposits. Econ. Geol. 93, 564–586.

Buchanan, P.C., Reimold, W.U., Koeberl, C., Kruger, F.J., 2004. Rb–Sr and Sm–Nd isotopic compositions of the Rooiberg Group, South Africa: early Bushveld-related volcanism. Lithos 29, 373–388.

Buick, I.S., Lana, C., Gregory, C., 2011. A LA-ICP-MS and SHRIMP U/Pb age constraint on the timing of REE mineralization associated with Bushveld granites. S. Afr. J. Geol. 114 (1), 1–14.

Constantopoulos, J., 1988. Fluid inclusions and rare earth element geochemistry of fluorite from South-Central Idaho. Econ. Geol. 83, 626–636.

Corvino, A.F., Henjes-Kunst, F., 2007. A record of 2.5 and 1.1 billion year old crust in the Lawrence Hills, Antarctic Southern Prince Charles Mountains. Terra Antact. 14 (1), 13–30.

Crocker, I.T., 1985. Volcanogenic fluorite–hematite deposits and associated pyroclastic rock suite at Vergenoeg, Bushveld Complex. Econ. Geol. 80, 1181–1200.

Crocker, I.T., Martini, J.E.J., Söhnge, A.P.G., 1988. The fluorspar deposits of the Republics of South Africa and Bophuthatswana. Handbook of the Geological Survey, Department of Mineral and Energy Affairs, South Africa (172 pp.).

Crocker, I.T., Eales, H.V., Ehlers, D.I., 2001. Fluorite, Cassiterite and Sulphide Deposits Associated with the Acid Rocks of the Bushveld Complex. Memoir of the Council for Geosciences, South Africa (151 pp.).

Dorland, H.C., Beukes, N.J., Gutzmer, J., Evans, D.A.D., Armstrong, R.A., 2006. Precise SHRIMP U–Pb zircon age constraints on the lower Waterberg and Soutpansberg Groups, South Africa. S. Afr. J. Geol. 109, 139–156.

Ercit, T.S., 2005. Identification and alteration trends of granitic-pegmatite-hosted (Y, REE, U, Th)–(Nb, Ta, Ti) oxide minerals: a statistical approach. Can. Mineral. 43, 1291–1303.

Eriksson, P.G., Hattingh, P.J., Altermann, W., 1995. An overview of the geology of the Transvaal Sequence and Bushveld Complex, South Africa. Miner. Deposita 36, 98–111.

Estrada, S., Henjes-Kunst, F., Burgath, K.-P., Roland, N.W., Schäfer, F., Khain, E.V., Remizov, D.N., 2012. Insights into the magmatic and geotectonic history of the Voikar Massif, Polar Urals. Z. D. G. G. 163, 9–41.

Förster, H.-J., 1998. The chemical composition of REE–Y–Th–U-rich accessory minerals in peraluminous granites of the Erzgebirge–Fichtelgebirge region, Germany. Part II: xenotime. Am. Mineral. 93, 564–586.

Fourie, P.J., 2000. The Vergenoeg fayalite iron oxide fluorite deposit, South Africa: some new aspects. In: Porter, T.M. (Ed.), Hydrothermal Iron Oxide Copper–Gold and Related Deposits a Global Perspective. Australian Mineral Foundation, Adelaide, pp. 309–320.

Giere, R., 1996. Formation of rare earth minerals in hydrothermal systems. In: Jones, A.P., et al. (Eds.), Rare Earth Minerals: Chemistry, Origin and Ore Deposits. Chapman and Hall, London, pp. 105–150.

Goff, B.H., Weinberg, R., Groves, D.I., Vielreicher, N.M., Fourie, P.J., 2004. The giant Vergenoeg fluorite deposit in a magnetite–fluorite–fayalite REE pipe: a hydrothermal-altered carbonatite-related pegmatoid? Mineral. Petrol. 80, 173–199.

Graupner, T., Melcher, F., Gäbler, H.-E., Sitnikova, M., Brätz, H., Bahr, A., 2010. Rare earth element geochemistry of columbite-group minerals: LA–ICP-MS data. Mineral. Mag. 74, 691–713.

Harlov, D.E., Förster, H.-J., 2003. Fluid-induced nucleation of (Y + REE)-phosphate minerals within apatite: nature and experiment, part II. Fluorapatite. Am. Mineral. 88, 1209–1229.

Harlov, D.E., Anderson, U.B., Förster, H.-J., Nyström, J.O., Dulski, P., Broman, C., 2002. Apatite–monazite relations in the Kiirunavaara magnetite–apatite ore, northern Sweden. Chem. Geol. 191, 47–72.

Harmer, R.E., Armstrong, R.A., 2000. Duration of Bushveld Complex (sensu lato) magmatism: constraints from new SHRIMP zircon chronology. Abstract Workshop on the Bushveld Complex, 18–21 November 2000. Gethlane Lodge, Burgersfort, South Africa.

Hill, M., Barker, F., Hunter, D., Knight, R., 1996. Geochemical characteristics and origin of the Lebowa Granite Suite, Bushveld Complex. Int. Geol. Rev. 38, 195–227.

Jacobsen, S.B., Wasserburg, G.J., 1980. Sm–Nd isotopic evolution of chondrites. Earth Planet. Sci. Lett. 50, 139–155.

Kinnaird, J.A., Kruger, F.J., Cawthorn, R.G., 2004. Rb–Sr and Nd–Sm isotopes in fluorite related to the granites of the Bushveld Complex. S. Afr. J. Geol. 107, 413–430.

Ludwig, K.R., 2008. User's manual for Isoplot 3.6: a geochronological toolkit for Microsoft Excel. Special Publication, 4. Berkeley Geochronology Center, Berkeley (77 pp.).

McDonough, W.F., Sun, S.-s., 1995. Composition of the earth. Chem. Geol. 120, 223–253.

McNaughton, N.J., Pollard, P.J., Groves, D.I., Taylor, R.G., 1993. A long-lived hydrothermal system in Bushveld granites at the Zaaiplaats tin mine: lead isotope evidence. Econ. Geol. 88, 27–43.

Möller, P., Parekh, P.P., Schneider, H.-J., 1976. The application of Tb/Ca–Tb/La abundance ratios to problems of fluorspar genesis. Mineral. Deposita 11, 111–116.

Neuser, R.D., Bruhn, F., Götze, J., Habermann, D., Richter, D.K., 1995. Cathodoluminescence: methods and application. Zbl. Geol. Paläontol. 1/2, 287–306.

Ngwenya, B.T., 1994. Hydrothermal rare earth mineralization in carbonatites of the Tundulu complex, Malawi: process at the fluid/rock interface. Geochim. Cosmochim. Acta 58, 2061–2072.

Pan, Y., Fleet, M.E., Barnett, R.L., Chen, Y., 1993. Pyrosmalite in Canadian Precambrian sulfide deposits: mineral chemistry, petrogenesis and significance. Can. Mineral. 31, 695–710.

Pearce, N.J.G., Perkins, W.T., Westgate, J.A., Gorton, M.P., Jackson, S.E., Neal, C.R., Chenery, S.P., 1997. A compilation of new and published major and trace element data for NIST SRM 610 and NIST SRM 612 glass reference materials. Geostand. Newslett. 21, 115–144.

Rajesh, H.M., Chisonga, B.C., Shindo, K., Beukes, N.J., Armstrong, R.A., 2013. Petrographic, geochemical and SHRIMP U–Pb titanite age characterization of the Thabazimbi mafic sills: extended time frame and a unifying petrogenetic model for the Bushveld Large Igneous Province. Precambrian Res. 230, 79–102.

Rasmussen, M.G., Evans, B.W., Kuehner, S.M., 1998. Low-temperature fayalite, greenalite, and minnesotaite from the Overlook gold deposit, Washington: phase relations in the system FeO–SiO_2–H_2O. Can. Mineral. 36, 147–162.

Ruberti, E., Enrich, G.E.R., Gomes, C.B., Comin-Chiaramonti, P., 2008. Hydrothermal REE fluorocarbonate mineralization at Barra do Itapirapua, a multiple stockwork carbonatite, Southern Brazil. Can. Mineral. 46, 901–914.

Scherhag, C., 1990. Flußspat-Lagerstätten in Südafrika - ein Überblick. Erzmetall 43, 28–33.

Schütte, P., 2005. Investigations on the Genesis of the Vergenoeg Fe–F Deposit, RSA. (Diploma thesis) University of Hannover, Germany (162 pp.).

Scoates, J.S., Wall, C.J., Friedman, R.M., VanTongeren, J.A., Mathez, E.A., 2012. Age of the Bushveld Complex. Goldschmidt 2012 Conference Abstracts. Mineral. Mag. 76, 2348.

Škoda, R., Novák, M., Cicha, J., 2011. Uranium–niobium-rich alteration products after "písekite", an intimate mixture of Y, REE, Nb, Ta, Ti-oxide minerals from the Obrázek I pegmatite, Písek, Czech Republic. J. Geosci. 56, 317–325.

Torab, F.M., Lehmann, B., 2007. Magnetite–apatite deposits of the Bafq district, Central Iran: apatite geochemistry and monazite geochronology. Mineral. Mag. 71, 347–363.

Wall, F., Williams, C.T., Woolley, A.R., 1996. Pyrochlor from weathered carbonatite at Lueshe, Zaire. Mineral. Mag. 60, 731–750.

Walraven, F., 1997. Geochronology of the Rooiberg Group. Transvaal Supergroup, South Africa. EGRI Information Circular, 316. University of the Witswatersrand (216 pp.).

Walraven, F., Hattingh, E., 1993. Geochronology of the Nebo Granite, Bushveld Complex. S. Afr. J. Geol. 96, 31–41.

Watson, E.B., 1976. Two-liquid partition coefficients: experimental data and geochemical implications. Contrib. Mineral. Petrol. 56, 119–134.

Williams-Jones, A.E., Wood, S.A., 1992. A preliminary petrogenetic grid for REE fluorocarbonates and associated minerals. Geochim. Cosmochim. Acta 56, 725–738.

Wood, S.A., Samson, I.M., 2000. The hydrothermal geochemistry of tungsten in granitoid environments: I. Relative solubilities of ferberite and scheelite as a function of T, P, pH, and mNaCl. Econ. Geol. 95, 143–182.

Please cite this article as: Graupner, T., et al., Mineralogy of high-field-strength elements (Y, Nb, REE) in the world-class Vergenoeg fluorite deposit, South Africa, Ore Geol. Rev. (2014), http://dx.doi.org/10.1016/j.oregeorev.2014.02.012